EPRI | ELECTRIC POWER RESEARCH INSTITUTE

The Grades 11 and 12 Low Alloy Steel Handbook

1¼Cr½Mo, 1Cr½Mo, 13CrMo44, 620/621, STPA 22/23

The Grades 11 and 12 Low Alloy Steel Handbook

1¼Cr½Mo, 1Cr½Mo, 13CrMo44, 620/621, STPA 22/23

1013358

Final Report, March 2007

EPRI Project Manager
D. Gandy

ELECTRIC POWER RESEARCH INSTITUTE
3420 Hillview Avenue, Palo Alto, California 94304-1338
PO Box 10412, Palo Alto, California 94303-0813 ▪ USA
800.313.3774 ▪ 650.855.2121 ▪ askepri@epri.com ▪ www.epri.com

DISCLAIMER OF WARRANTIES AND LIMITATION OF LIABILITIES

ORGANIZATION(S) THAT PREPARED THIS DOCUMENT

Structural Integrity Associates, Inc.

NOTE

For further information about EPRI, call the EPRI Customer Assistance Center at 800.313.3774 or e-mail askepri@epri.com.

CITATIONS

This report was prepared by:

Structural Integrity Associates, Inc.
2904 South Sheridan Way, Suite 303
Oakville, Ontario L6J 7L7, Canada

Principal Investigator
J. Parker

This report describes research sponsored by the Electric Power Research Institute (EPRI).

The report is a corporate document that should be cited in the literature in the following manner:

The Grades 11 and 12 Low Alloy Steel Handbook: 1¼Cr½Mo, 1Cr½Mo, 13CrMo44, 620/621, STPA 22/23. EPRI, Palo Alto, CA: 2007. 1013358.

PRODUCT DESCRIPTION

The design conditions of different fossil power boilers vary, and in a large power generating system, many different alloys can be used in various product forms. Although specifications and standards apply to these alloys, utility engineers frequently need basic metallurgical information to guide them in making decisions for specific projects. The topic of this report—part of an ongoing series of metallurgical handbooks developed under the EPRI Fossil Materials and Repair Program (Program 87)—is Grade 11 and Grade 12 steels.

Results and Findings

This report concentrates on several key aspects of Grade 11 (1¼Cr½Mo) and Grade 12 (1Cr½Mo) steels (including the equivalent German [13CrMo4 4], British [620/621], and Japanese [STPA 22/23] steels). Among the topics discussed are standards and codes, metallurgy (microstructure and properties), mechanical properties (new and service-exposed), oxidation resistance, and fabrication and welding.

Challenges and Objectives

Maintaining an accurate knowledge of the full range of boiler materials has become increasingly challenging: even for well-established alloys, the information base continues to expand, and new alloys with complex metallurgies are being introduced. The intent of this report and the others in the series is to provide a comprehensive materials reference that organizes relevant information in a concise manner for each material.

Applications, Value, and Use

The content and organization of this report have been chosen to assist utility metallurgists, welding engineers, and maintenance personnel in addressing materials, metallurgy, and mechanical properties issues related to Grade 11 and Grade 12 steels. To give it the convenient portability of a field guide, this report has been formatted as a pocket handbook.

EPRI Perspective

This report and the others in the series provide information about the most common boiler materials. Although each has been produced as a volume on an individual alloy, a broader perspective of the metallurgical aspects of boiler steels can be gained through the EPRI report *Metallurgical Guidebook for Fossil Power Plant Boilers* (1011912). Readers might also wish to consult the previous report in this series—*The Grade 22 Low Alloy Steel Handbook* (1011534).

Approach

This report is one of a series of metallurgical handbooks being developed for several major component materials used in fossil power production. In each section of these reports, the project team has presented information in a succinct manner, with references to source documents supporting technical information.

Keywords

Fabrication issues
Fossil materials and repair
Metallurgy
Standards and codes
Welding issues

ABSTRACT

A series of metallurgical reports is being developed for several of the major component materials currently used in fossil power production under the EPRI Fossil Materials and Repair Program. The intent of the series is to provide a comprehensive materials source that organizes relevant information in a succinct manner for each individual material. The present report has been developed specifically for Grades 11 and 12 (1¼Cr½Mo and 1Cr½Mo) steels and is geared to assist utility metallurgists, welding engineers, and maintenance personnel in addressing materials metallurgy and mechanical properties issues surrounding this material. The report focuses on several key areas, including standards and codes, metallurgy, mechanical properties (new and service-exposed), and fabrication and welding issues.

CONTENTS

1 **INTRODUCTION** **1-1**

2 **TECHNICAL BACKGROUND** **2-1**

2.1 Forms Available 2-2

2.2 Applications 2-2

3 **STANDARDS AND CODES** **3-1**

3.1 ASME Boiler and Pressure Vessel Code Specifications 3-1

3.2 Allowable Stresses 3-5

4 **METALLURGY** **4-1**

4.1 Chemical Composition 4-1

4.2 Microstructure and Heat Treatment 4-7

4.2.1 Transformation Behavior 4-7

4.2.2 Time Temperature Transformation Diagram 4-7

4.2.3 Continuous Cooling Diagram 4-8

4.2.4 Final Heat Treatment 4-12

4.2.5 Microstructure 4-13

4.2.6 Carbides in CrMo Low Alloy Steels 4-15

4.2.7 Hardness Changes 4-20

5 **PROPERTIES** **5-1**

5.1 Physical Properties 5-1

5.2 Tensile and Yield Strength 5-7

5.3 Creep Properties 5-8

5.3.1 Representations with Stress and Temperature 5-12

5.3.2 Creep Rupture 5-14

5.4 Creep Crack Growth 5-22

5.5 Fatigue Properties 5-25

5.5.1 Fatigue Crack Growth 5-27

5.6 Creep Fatigue Behavior 5-28

5.6.1 Creep Fatigue Crack Growth 5-30

5.7 Toughness 5-32

5.8 Aging Effects on Properties 5-34
5.8.1 Carbide Embrittlement 5-35
5.8.2 Temper Embrittlement 5-35

***6* OXIDATION RESISTANCE 6-1**
6.1 Scale Formation 6-1
6.2 Growth of Laminated Scales 6-3
6.3 Oxidation Rate of 1¼CrMo Steels in Steam 6-3
6.4 Life Assessment by Oxide Thickness Measurements 6-6
6.4.1 Metallographic Measurement of Steam-Side Scales 6-7
6.4.2 Ultrasonic Measurement of Oxide Scales 6-8

***7* FABRICATION ISSUES 7-1**
7.1 Workability and Forming 7-1
7.2 Welding 7-6
7.2.1 Welding Processes and Consumables 7-6
7.2.2 Welding PWHT 7-6
7.2.3 Weld Procedure Selection 7-8
7.2.4 Weld Joint Preparation 7-11
7.2.5 Repair Pipe and Fitting Weld Repair and Replacement 7-13

***8* REFERENCES 8-1**

LIST OF FIGURES

Figure 3-1 Comparison of the ASME Code Allowable Stresses in Different Years for Grade 11 Steel 3-6

Figure 4-1 Typical TTT Diagram for Grade 11 Low Alloy Steel 4-8

Figure 4-2 Typical CCT Diagram for Grade 11 Low Alloy Steel 4-9

Figure 4-3 Typical Microstructures in Grade 12 Low Alloy Steel Showing Typical Ferrite and Pearlite Microstructure 4-11

Figure 4-4 Typical Microstructure Observed in a Grade 11 Low Alloy Steel Weldment 4-12

Figure 4-5 Macrosection Showing Grade 11 Weldment in Which the PWHT Involved Subcritical Heating 4-15

Figure 4-6 Optical Micrographs from a Section of T12 Superheater Tubing After Long-Term Service Showing the Precipitate Coarsening 4-16

Figure 4-7 Detailed Electron Micrograph Showing the Typical Distribution of Carbides in Grade 12 Low Alloy Steel After Long-Term Service at Around 550ºC (1022ºF) 4-17

Figure 4-8 Detailed Measurements Showing the Coarsening of Carbides in Grade 12 Steel for Different Temperatures 4-18

Figure 4-9 A Set of Optical Micrographs Illustrating the Microstructural Changes in 1CrMo Low Alloy Steel After Long-Term Service at Around 550ºC (1022ºF) 4-19

Figure 4-10 Reductions in Hardness in CrMo Steel as a Function of Time at Temperature Given by the Hollomon-Jaffe Parameter 4-21

Figure 5-1 Variation in the Elastic Modulus with Temperature 5-3

Figure 5-2 Variation in (a) Poisson's Ratio and (b) Thermal Conductivity with Temperature 5-5

Figure 5-3 Variation in Thermal Diffusivity with Temperature 5-6

Figure 5-4 Variation in the Instantaneous Coefficient of Linear Thermal Expansion at the Indicated Temperatures 5-6

Figure 5-5 Variation in Yield Strength, Tensile Strength, Average Creep Strength, and Average 100,000 Hours Rupture Strength with Temperature for Grade 12 Material Heat-Treated in the Annealed Condition 5-7

Figure 5-6 Variation in Yield Strength, Tensile Strength, Average Creep Strength, and Average 100,000 Hours Rupture Strength with Temperature for Grade 11 Material Heat-Treated in the Annealed Condition 5-8

Figure 5-7 A Comparison of Creep Rupture Strengths in Grade 11 and Grade 12 Steels 5-9
Figure 5-8a Variation in the Larson-Miller Parameter with Applied Stress for Grade 12 Steel 5-10
Figure 5-8b Variation in the Larson-Miller Parameter with Applied Stress for Grade 11 Steel 5-11
Figure 5-9 Combinations of Stress and Temperature Yielding a Range of Creep Lives 5-13
Figure 5-10 Creep Void Development in 1¼Cr¼Mo Steel Shown in an Optical Micrograph 5-15
Figure 5-11 Alignment of Creep Voids Indicative of Damage Close to Microcrack Initiation 5-15
Figure 5-12 Creep Cavities Formed in the Intercritical (Type IV) Region of a Weld HAZ (a) and in the Weld Metal (b) 5-16
Figure 5-13 A Semi-Quantitative Relationship Between Creep Cavity Classification and Life Fraction 5-17
Figure 5-14 Relationship for Grade 12 Steel and Other Boiler Steels Showing the Number Fraction of Grain Boundaries with Creep Voids Present and Life Fraction 5-18
Figure 5-15 Description of Damage Development with Life Fraction for Grade 12 5-19
Figure 5-16 Variation in Reduction in Area at Fracture with Applied Stress for Creep Tests on Grade 11 Steel 5-20
Figure 5-17 Relationship Between the Average Elongation Rate and Rupture Life for Creep Tests on Grade 11 Steel 5-21
Figure 5-18 Isoductility Contours with Different Rupture Lives for Grade 11 Steel 5-22
Figure 5-19 Average Creep Crack Growth Rate for Grade 11 Parent at 1000ºF 5-23
Figure 5-20 Comparison of Crack Growth Rate Scatter Bands for Ex-Service HAZ/Fusion Line Material and Base Material 5-25
Figure 5-21 Variation in Cycles to Failure with Strain for High-Temperature Fatigue 5-27
Figure 5-22 Fatigue Crack Growth Behavior 5-28
Figure 5-23 Test Results for Grade 11 Steel Showing That Holding at High Temperature Significantly Reduced the Number of Cycles to Failure 5-29
Figure 5-24 Creep Fatigue Interaction Diagram Showing That Linear Damage Estimates Significantly Overestimate Component Life 5-30
Figure 5-25 Effect of Increasing Temperature on the Cyclic Crack Growth Rate for a Range of Alloys Used in Elevated Temperature and Pressure Applications 5-31
Figure 5-26 Master Curve Approach Relating FATT with Fracture Toughness for Grade 11 Steel 5-33
Figure 5-27 Measured Values of FATT for Different Times of Exposure at Elevated Temperature for 1CrMo Steels 5-36

Figure 6-1 Data Showing How Steam-Side Scale Growth Varies with Temperature for Boiler Alloys with Different Compositions of Cr 6-2
Figure 6-2 Typical Micrograph Showing Laminated Steam-Side Scale Developed on a CrMo Tube 6-2
Figure 6-3 Summary of the Oxide Growth Constant for Iron, Carbon, and Alloy Steels 6-5
Figure 6-4 Typical Ex-Service Tube Showing the Buildup of Scale and Wall Loss at the 10 O'Clock and 2 O'Clock Positions 6-7
Figure 7-1 Groove Weld End Preparation Nomenclature 7-12
Figure 7-2 Open Root Joint Details 7-13
Figure 7-3 Excavations for Defect Type Verification and Local Weld Repair 7-15
Figure 7-4 Cavity Fill Sequence for Local Weld Repair 7-16
Figure 7-5 Cavity Fill Sequence for Full Weld Replacement 7-18

LIST OF TABLES

Table 2-1 Examples of International Specifications for Grade 11 Steel 2-1
Table 2-2 Examples of International Specifications for Grade 12 Steel 2-1
Table 2-3 Peak Temperatures Recommended by Code and Manufacturers 2-2
Table 3-1 Selected Specifications for Grade 11 Steel According to ASME Boiler and Pressure Vessel Code 3-2
Table 3-2 Selected Specifications for Grade 12 Steel According to ASME Boiler and Pressure Vessel Code 3-4
Table 3-3 Allowable Stress Values in ksi for Metal Temperatures According to Section I of the ASME Boiler and Pressure Vessel Code 3-5
Table 3-4 Maximum Allowable Design Stress Values in MPa for Grade 12 Steel Pipes for Metal Temperatures According to BS 806 3-7
Table 3-5 Maximum Allowable Design Stress Values in MPa for Grade 11 Steel Pipes for Metal Temperatures According to BS 806 3-7
Table 3-6 Maximum Allowable Mean Stress Values in MPa for Grade 12 Steel Tube Metal Temperatures According to DIN 17175-79..... 3-7
Table 4-1 Composition of Grade 11 Low Alloy Steels According to ASME SA-213 and ASME SA-335 as Compared to European and Japanese Standards 4-2
Table 4-2 Composition of Grade 12 Low Alloy Steels According to ASME SA-213 and ASME SA-335 as Compared to European and Japanese Standards 4-3
Table 4-3 Composition of Grade 11 and Grade 12 Low Alloy Steels According to ASME Codes..... 4-5
Table 4-4 Influence of Cooling Rate on Microstructure and Hardness 4-10
Table 5-1 Typical Physical Properties at Room Temperature 5-2
Table 5-2 Variation in Selected Physical Properties with Temperature..... 5-4
Table 5-3 Combinations of Stress and Temperature Yielding a Range of Creep Lives 5-14
Table 5-4 Summary of Creep Crack Growth Constants for Equation 5-7..... 5-24
Table 5-5 Chemical Compositions of Materials (by Percentage Weight) 5-37
Table 6-1 Maximum Tube Metal Temperatures 6-1
Table 7-1 Guidance on Post-Forming Heat Treatments for Bends in Grade 11 and 12 Tubes..... 7-4

Table 7-2 Recommended PWHT Requirements for High-Temperature Piping Materials 7-7
Table 7-3 Summary of Designated Weld P Numbers for Selected Alloy Steels 7-10

1
INTRODUCTION

The components in power boilers and the associated piping are involved in the following functions:

- Generating steam
- Increasing steam temperature and pressure
- Moving water and steam

Because the tubing and piping systems are multifunctional and operate at different pressures and temperatures, it is reasonable that the components involved are manufactured from different alloys using a range of fabrication techniques. Moreover, because the design conditions of different boilers vary within a broad power-generating system, many different alloys will be used in various product forms. The materials used and the associated product quality checks are covered by applicable specifications and standards. However, it is frequently necessary for utility engineers to have access to basic metallurgical information to aid decision making for specific projects. Maintaining accurate knowledge of the full range of boiler materials is becoming an increasing challenge for two main reasons: the information base continues to grow even for well-established alloys, and new alloys—many with complex metallurgy—are being introduced.

This series of reports has been developed to provide information regarding the most common boiler materials. Each report has been produced for an individual alloy; however, in order to gain a full appreciation for the metallurgical aspects of boiler steels, reference should also be made to the EPRI report *Metallurgical Guidebook for Fossil Power Plant Boilers* [1].

To facilitate the extraction of information, each volume in the series has been prepared using a similar format, with information presented on the following:

- Metallurgy covering microstructure and properties
- Standards and codes
- Fabrication issues

In each section, information of benefit to utility engineers is presented in a succinct manner and supported by appropriate references to source documentation.

2
TECHNICAL BACKGROUND

Steels based on chromium (Cr) and molybdenum (Mo) are widely used in boilers and piping, and 1¼Cr½Mo (Grade 11) and 1Cr½Mo (Grade 12) low alloy steels have been standardized in countries across the world for more than 50 years [2]. Grade 12 steels are most commonly used in Europe and Japan, with the Grade 11 most commonly used in North America. Grade 11 alloy contains up to 1% silicon (Si) and is sometimes identified as 1¼Cr½MoSi. The high Si level in Grade 11 steel is added for better oxidation, scaling, and fireside corrosion resistance, which is particularly important in tubing. Example specification numbers from the United States (as specified by ASTM International [ASTM]), UK, Germany (as specified by Deutsches Institut fur Normung [DIN]), and Japan are given in Tables 2-1 and 2-2.

Table 2-1
Examples of International Specifications for Grade 11 Steel

ASTM	British	German	Japanese
SA-213 T11	3606 S1 621	_	G 3462 STBA23
SA-335-P11	3604 CFS621	_	G 3458 STPA23

Table 2-2
Examples of International Specifications for Grade 12 Steel

ASTM	British	German	Japanese
SA-213 T12	3606 S1 620	DIN 28180 13CrMo44	G 3462 STBA22
SA-335-P12	3604 CFS620	DIN 17175 13CrMo44	G 3458 STPA22

The alloys now widely known as *Grades 11 and 12* based on the ASTM alloy designations have been used successfully in power plant applications that require reasonable high-temperature strength (derived primarily from a dispersion of fine Mo carbide precipitates) and resistance to oxidation (derived from the Cr present). The most common applications are in superheater and reheater tubing as well as high-temperature headers and piping where operation up to about 1112ºF (600ºC) is required. In fact, different codes and manufacturers recommend different peak temperatures for Grade 11 and Grade 12 steels. An example is shown in Table 2-3.

Table 2-3
Peak Temperatures Recommended by Code and Manufacturers

ASME Specification	ASME °F/°C	Babcock & Wilcox °F/°C	ALSTOM °F/°C	Riley °F/°C
SA-213 T11	1200/649	1050/566	1025/552	1025/552

Experience suggests that for excellent long-term performance, the sustained metal temperature should be below about 1050ºF (566ºC); however, it is apparent that the specific information regarding pressure, temperature, and environment should be considered when selecting material and component geometry.

2.1 Forms Available

Grade 11 and 12 alloys are available in the following forms:

- Tubes
- Pipes
- Forgings
- Castings
- Bars
- Rods
- Plates
- Sheets

2.2 Applications

Grade 11 and 12 alloys are used in the following applications:

- High-pressure boilers
- Superheaters
- Drying ovens
- Air preheaters
- Incinerators
- Heat exchangers
- Other high-temperature service where good creep strength or resistance to corrosion and oxidations or both is desired

3
STANDARDS AND CODES

3.1 ASME Boiler and Pressure Vessel Code Specifications

Selected American Society of Mechanical Engineers (ASME) specifications for Grade 11 and Grade 12 steels are listed in Tables 3-1 and 3-2, respectively. Tables 3-1 and 3-2 also include applicable product forms and room-temperature mechanical property requirements. Strength is expressed in kips per square inch (ksi) and megapascals (MPa).

Table 3-1
Selected Specifications for Grade 11 Steel According to ASME Boiler and Pressure Vessel Code

ASME Specification	Grade	Product Form	Mechanical Properties						
			Minimum Yield Strength (ksi)	Minimum Yield Strength (MPa)	Minimum Tensile Strength (ksi)	Minimum Tensile Strength (MPa)	Elongation (%)	Reduction of Area (%)	Hardness (H_b)
SA-182	F11 Class 1	Forging	30	205	60	413	20	45	121–174
SA-182	F11 Class 2	Forging	40	275	70	485	20	30	143–207
SA-182	F11 Class 3	Forging	45	310	75	515	20	30	156–207
SA-213	T11	Tube	30	205	60	410	22	-	163 maximum
SA-217	WC6	Casting	40	275	70–95	485–655	20	35	-
SA-217	WC11	Casting	50	345	80–105	550–725	18	45	-
SA-335	P11	Pipe	30	205	60	415	22	-	-
SA-336	F11 Class 1	Forging	30	205	60–85	415–585	20	45	-

Table 3-1 (continued)
Selected Specifications for Grade 11 Steel According to ASME Boiler and Pressure Vessel Code

ASME Specification	Grade	Product Form	Mechanical Properties						
			Minimum Yield Strength (ksi)	Minimum Yield Strength (MPa)	Minimum Tensile Strength (ksi)	Minimum Tensile Strength (MPa)	Elongation (%)	Reduction of Area (%)	Hardness (H_b)
SA-336	F11 Class 2	Forging	40	275	70–95	485–660	20	40	-
SA-336	F11 Class 3	Forging	45	310	75–100	515–690	18	40	-
SA-369	F11	Forging	30	205	60	410	22	-	-
SA-387	11 Class 1	Plate	35	241	60–85	415–585	22	-	-
SA-387	11 Class 2	Plate	45	310	75–100	515–690	22	-	-

Table 3-2
Selected Specifications for Grade 12 Steel According to ASME Boiler and Pressure Vessel Code

ASME Specification	Grade	Product Form	Mechanical Properties						
			Minimum Yield Strength (ksi)	Minimum Yield Strength (MPa)	Minimum Tensile Strength (ksi)	Minimum Tensile Strength (MPa)	Elongation (%)	Reduction of Area (%)	Hardness (H_b)
SA-182	F12 Class 1	Forging	32	220	60	415	20	45	121–174
SA-182	F12 Class 2	Forging	40	275	70	485	20	30	143–207
SA-213	T12	Tube	32	220	60	415	22	-	163 maximum
SA-335	P12	Pipe	32	220	60	415	22	-	-
SA-336	F12	Forging	40	275	70–95	485–660	20	40	-
SA-369	F12	Forging	32	220	60	415	22	-	-
SA-387	12 Class 1	Plate	33	228	55–80	380–550	22	-	-
SA-387	12 Class 2	Plate	40	275	65–85	450–585	22	-	-

3.2 Allowable Stresses

The allowable stress values given in U.S. and UK codes are presented in Tables 3-3 through 3-6. Because of a difference in design philosophy, the British Standards (BS) code recommends different allowable stress values for different anticipated operating lives.

Table 3-3
Allowable Stress Values in ksi for Metal Temperatures According to Section I of the ASME Boiler and Pressure Vessel Code

ASME Code	Temperature (°F/°C)										
	700/ 371	750/ 399	800/ 427	850/ 454	900/ 482	950/ 510	1000/ 538	1050/ 566	1100/ 593	1150/ 621	1200/ 649
SA 213 T11 SA 182 F11 SA 336 F11 Class 1	15.1	14.8	14.4	14.0	13.6	9.3	6.3	4.2	2.8	1.9	1.2
SA 336 F11 Class 2	20	19.7	19.2	18.7	13.7	9.3	6.3	4.2	2.8	1.9	1.2
SA 336 F11 Class 3	21.4	21.4	21.4	20.2	13.7	9.3	6.3	4.2	2.8	1.9	1.2
SA 213 T12 SA 182 F12	15.8	15.5	15.3	14.9	14.5	11.3	7.2	4.5	2.8	1.8	1.1

1 ksi = 6.895 MPa

It should be noted that the ASME allowable stresses for Grade 11 alloys operating at temperatures above 950ºF (510ºC) (such as under creep conditions) were reduced in the 1980 version of the Code. Equipment that is still in operation and designed before 1980 should be examined for evidence of high-temperature damage because, as shown in Figure 3-1, the reductions in stress were significant.

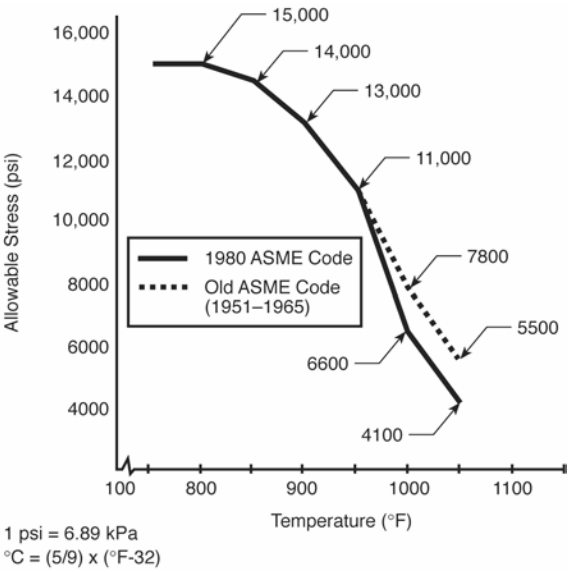

Figure 3-1
Comparison of the ASME Code Allowable Stresses in Different Years for Grade 11 Steel

Table 3-4
Maximum Allowable Design Stress Values in MPa for Grade 12 Steel Pipes for Metal Temperatures According to BS 806

Design Life (hr)	Design Temperature (°C)							
	250	300	350	400	450	500	550	570
100,000	157	128	121	116	112	111	42	27
150,000						102	35	24
200,000						94	32	22
250,000						88	30	20

Table 3-5
Maximum Allowable Design Stress Values in MPa for Grade 11 Steel Pipes for Metal Temperatures According to BS 806

Design Life (hr)	Design Temperature (°C)							
	250	300	350	400	450	500	550	570
100,000	145	116	110	105	101	100	42	27
150,000						100	35	24
200,000						94	32	22
250,000						88	30	20

Table 3-6
Maximum Allowable Mean Stress Values in MPa for Grade 12 Steel Tube Metal Temperatures According to DIN 17175-79 (Minimum values are typically about 20% lower than the mean.)

Design Life (hr)	Temperature (°C)							
	250	300	350	400	450	500	550	570
10,000					370	239	109	24
100,000					285	137	49	33
200,000					260	115	39	26

4
METALLURGY

4.1 Chemical Composition

The chemical compositions of Grade 11 steel specified by ASME SA-213 T11 and ASME SA-335 P11 and similar UK and Japanese steels given in the ASTM's *Handbook of Comparative World Steel Standards* [3] are compared in Table 4-1. (In Japan, the Japanese Standards Association establishes the Japanese Industrial Standards [JISs].) The compositions of Grade 12 steels obtained from similar sources are compared in Table 4-2. The basic requirements have changed little since the introduction of these steels more than 50 years ago. However, improvements in steel making practice have allowed greater control of trace elements, such as phosphorus and sulfur.

Table 4-1
Composition of Grade 11 Low Alloy Steels According to ASME SA-213 and ASME SA-335 as Compared to European and Japanese Standards

	ASTM SA 213 T11	BS 3606:92 621	JIS G 3462 STBA 23
Carbon	0.05–0.15	0.10–0.15	0.15 maximum
Manganese	0.30–0.60	0.30–0.60	0.30–0.60
Silicon	0.50–1.00	0.50–1.00	0.50–1.00
Phosphorus	0.025 maximum	0.040 maximum	0.030 maximum
Sulfur	0.025 maximum	0.040 maximum	0.030 maximum
Chromium	1.00–1.50	1.00–1.50	1.00–1.50
Nickel	-	0.30 maximum	-
Molybdenum	0.44–0.65	0.45–0.65	0.45–0.65
Others	-	Aluminum 0.020 maximum	-
	ASTM SA 335 P11	**BS 3604 621**	**JIS G 3458 STPA 23**
Carbon	0.05–0.15	0.15 maximum	0.15 maximum
Manganese	0.30–0.60	0.30–0.60	0.30–0.60
Silicon	0.50–1.00	0.50–1.00	0.50–1.00
Phosphorus	0.025 maximum	0.030 maximum	0.030 maximum
Sulfur	0.025 maximum	0.030 maximum	0.030 maximum
Chromium	1.00–1.50	1.00–1.50	1.00–1.50
Molybdenum	0.45–0.65	0.45–0.65	0.45–0.65
Others	-	Aluminum 0.02 maximum	-

Table 4-2
Composition of Grade 12 Low Alloy Steels According to ASME SA-213 and ASME SA-335 as Compared to European and Japanese Standards

	ASTM SA 213 T12	**BS 3059 620-460**	**JIS G 3462 STBA 22**	**DIN 28180:85 13CrMo4 4**
Carbon	0.05–0.15	0.10–0.15	0.15 maximum	0.10–0.18
Manganese	0.30–0.60	0.40–0.70	0.30–0.60	0.40–0.70
Silicon	0.50 maximum	0.10–0.35	0.50 maximum	0.10–0.35
Phosphorus	0.025 maximum	0.030 maximum	0.035 maximum	0.035 maximum
Sulfur	0.025 maximum	0.030 maximum	0.035 maximum	0.035 maximum
Chromium	0.80–1.25	0.70–1.10	0.80–1.25	0.70–1.10
Molybdenum	0.44–0.65	0.45–0.65	0.45–0.65	0.45–0.60
Others	S allowed to 0.045	Aluminum 0.020	-	-
	ASTM SA 335 P12	**BS 3604 620-440**	**JIS G 3458 STPA 22**	**DIN 17175:79 13CrMo4 4**
Carbon	0.05–0.15	0.10–0.15	0.15	0.10–0.18
Manganese	0.30–0.61	0.40–0.70	0.30–0.60	0.40–0.70
Silicon	0.50 maximum	0.10–0.35	0.50 maximum	0.10–0.35
Phosphorus	0.025 maximum	0.030 maximum	0.035 maximum	0.035 maximum
Sulfur	0.025 maximum	0.030 maximum	0.035 maximum	0.035 maximum
Chromium	0.80–1.25	0.70–1.10	0.80–1.25	0.70–1.10
Molybdenum	0.44–0.65	0.45–0.65	0.45–0.65	0.45–0.60
Others	-	Aluminum 0.02	-	Aluminum 0.02 Copper 0.30

The compositional specifications for the most commonly used ASTM specifications are compared in Table 4-3. The values given are those for product analysis. In most cases, the limits for Cr and Mo are similar; however, there are differences in ranges for carbon, manganese, and silicon and for the maximum allowable level of the trace elements phosphorus and sulfur.

Table 4-3
Composition of Grade 11 and Grade 12 Low Alloy Steels According to ASME Codes

Product Form	ASME or ASTM Specification	Grade	Composition (%)						
			Carbon	Manganese	Phosphorus	Sulfur	Silicon	Chromium	Molybdenum
Tubes	SA-213	T11	0.05–0.15	0.30–0.60	0.025 maximum	0.025 maximum	0.50–1.00	1.00–1.50	0.44–0.65
Pipe	SA-335	P11	0.05–0.15	0.30–0.60	0.025 maximum	0.025 maximum	0.50–1.00	1.00–1.50	0.44–0.65
Forgings	SA-336	F11	0.05–0.15	0.30–0.60	0.025 maximum	0.025 maximum	0.50–1.00	1.00–1.50	0.44–0.65
Forgings	SA-369	F11	0.05–0.15	0.30–0.60	0.025 maximum	0.025 maximum	0.50–1.00	1.00–1.50	0.44–0.65
Plate	SA-387	P11	0.04–0.17	0.35–0.73	0.035 maximum	0.035 maximum	0.44–0.86	0.94–1.56	0.40–0.70
Castings	SA-217	WC6	0.05–0.2	0.50–0.80	0.04 maximum	0.045 maximum	0.6 maximum	1.00–1.50	0.45–0.65

Table 4-3 (continued)
Composition of Grade 11 and Grade 12 Low Alloy Steels According to ASME Codes

Product Form	ASME or ASTM Specification	Grade	Composition (%)						
			Carbon	Manganese	Phosphorus	Sulfur	Silicon	Chromium	Molybdenum
Castings	SA-217	WC11	0.15–0.21	0.50–0.80	0.04 maximum	0.045 maximum	0.30–0.60	1.00–1.50	0.45–0.65
Tubes	SA-213	T12	0.05–0.15	0.30–0.60	0.025 maximum	0.025 maximum	0.50 maximum	0.80–1.25	0.44–0.65
Pipe	SA-335	P12	0.05–0.15	0.30–0.61	0.025 maximum	0.025 maximum	0.50 maximum	0.80–1.25	0.44–0.65
Forgings	SA-336	F12	0.10–0.20	0.30–0.80	0.025 maximum	0.025 maximum	0.10–0.60	0.80–1.10	0.45–0.65
Forgings	SA-369	F12	0.05–0.15	0.30–0.61	0.025 maximum	0.025 maximum	0.50 maximum	0.80–1.25	0.44–0.65
Plate	SA-387	P12	0.04–0.17	0.35–0.73	0.035 maximum	0.035 maximum	0.13–0.45	0.74–1.21	0.40–0.65

4.2 Microstructure and Heat Treatment

4.2.1 Transformation Behavior

Transformation temperatures are temperatures at which a change in phase occurs. The term is sometimes used to denote the limiting temperature of a transformation range. The following temperatures have been determined for studies of the behavior of Grade 11 steels:

- **AC_1**: The temperature at which austenite begins to form during heating is about 1430ºF (780ºC).
- **AC_3**: The temperature at which transformation of ferrite to austenite is completed during heating is about 1635ºF (890ºC).
- **AR_1**: The temperature at which transformation of austenite to ferrite or to ferrite plus cementite is completed during cooling is typically about 1285ºF (696ºC).
- **AR_3**: The temperature at which austenite begins to transform to ferrite during cooling is typically about 1550ºF (843ºC).
- **AR_4**: The temperature at which delta ferrite transforms to austenite during cooling.
- **B(s)**: The temperature at which transformation of austenite to bainite starts during cooling is typically about 1130ºF (611ºC).
- **M(s)**: The temperature at which transformation of austenite to martensite starts during cooling is typically about 810ºF (433ºC).
- **M(f)**: The temperature at which martensite formation finishes during cooling.

It should be emphasized that the time-dependent changes in phase occur at lower temperatures during cooling than during heating and depend on the rate of change in temperature.

4.2.2 Time Temperature Transformation Diagram

The microstructure depends on the composition and heat treatment history. Most often, slower cooling rates that are nearer to equilibrium result in the formation of ferrite and pearlite, with bainite or martensite formed under more rapid cooling conditions. Mixtures of these microstructures can also be formed. The particular microstructure formed

can be identified using time temperature transformation (TTT) diagrams. A typical TTT diagram for Grade 11 steel is shown in Figure 4-1. Because of the similar compositions for Grade 12 steels, the TTT diagram for this grade will be similar.

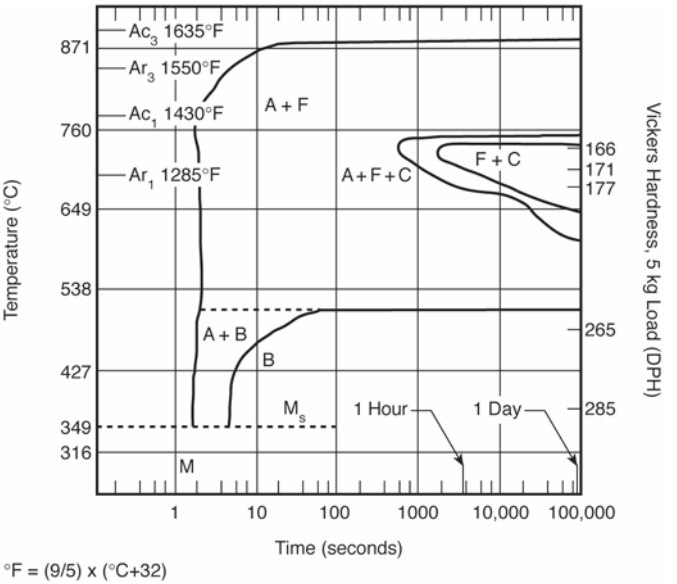

Figure 4-1
Typical TTT Diagram for Grade 11 Low Alloy Steel

4.2.3 Continuous Cooling Diagram

Similarly, continuous cooling transformation (CCT) curves are developed to show the microstructures formed through control of the applied thermal cycles for a number of different manufacturing processes. However, it is important that the thermal cycle used to produce the CCT curve be relevant to the particular process. One important factor to consider is the previous austenite grain size—that is, the grain size at the time of the first transformation from austenite. The previous austenite grain size has been shown to affect the transformation start temperature, or AR_3, for hot

rolling and annealing processes. For example, a ten-fold increase in the previous austenite grain size from 20 to 200 microns (μm) decreased the AR_3 temperature by about 50°C (122°F) at a cooling rate of 0.5°C/s (33ºF/s). However, this effect had reduced to a difference of only a few degrees at a cooling rate of 30°C/s (86ºF/s).

The microstructures expected following cooling from about 1750ºF (955ºC) can thus be estimated from the CCT diagram (see Figure 4-2). Very rapid quenching will produce predominantly martensitic structures; for cooling rates normally associated with boiler components, bainite formation will dominate at relatively rapid rates, with ferrite formation dominating during slow cooling. Typical examples of the microstructures formed are given in Table 4-4.

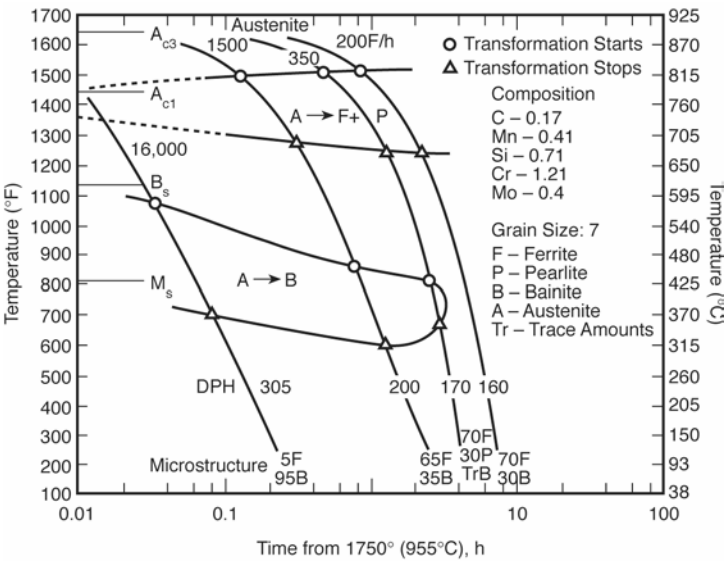

Figure 4-2
Typical CCT Diagram for Grade 11 Low Alloy Steel

Table 4-4
Influence of Cooling Rate on Microstructure and Hardness [2]

Cooling Rate (°F/hr/°C/hr)	Microstructure			Vickers Hardness
	Pearlite	Bainite	Ferrite	
16,000/8,871	0	95%	5%	305
1,500/816	0	65%	35%	215
350/177	~30%	Trace[1]	70%	170
200/93	30%	0	70%	160

[1]In the case of slow cooling, the transformation product can be pearlite with a trace of bainite.

In practical applications, slow cooling will often occur after heat treatment of large, thick section components, and in these components, largely ferritic microstructures are seen (see Figure 4-3). In most of these cases, the transformation product will be pearlite; however, at intermediate cooling rates, transformation to pearlite and bainite can occur. In these situations, the very fine lamella in the pearlite might not be easily resolved.

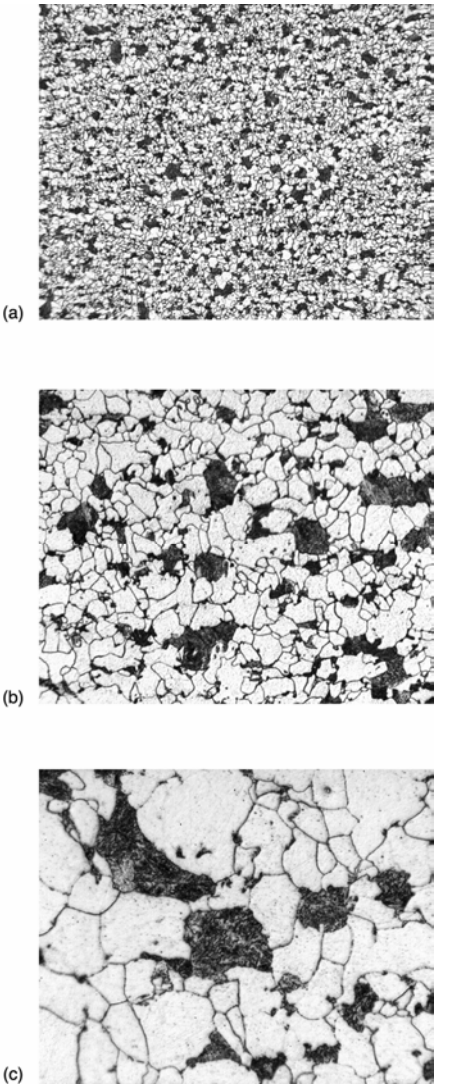

Figure 4-3
Typical Microstructures in Grade 12 Low Alloy Steel Showing Typical Ferrite and Pearlite Microstructure (Magnification for [a] is 50x, for [b] is 150x, and for [c] is 500x.)

In practical applications, fast cooling rates will usually be associated with welding so that the weld metal and heat-affected zone (HAZ) tend to exhibit bainitic microstructure (see Figure 4-4).

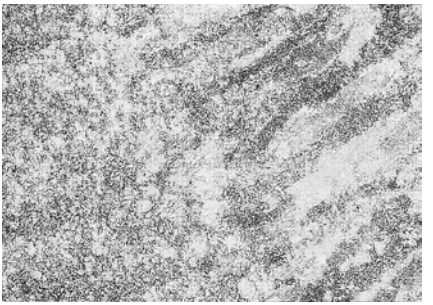

Figure 4-4
Typical Microstructure Observed in a Grade 11 Low Alloy Steel Weldment (The weld metal is toward the right; the HAZ is toward the left.) [4]

4.2.4 Final Heat Treatment

The austenitizing temperature for 1¼Cr1Mo steel is above about 990°C (1810°F). Heat treatments commonly employed with 1¼Cr1Mo steel include the following:

- Anneal. A full anneal involves austenitization at about 950°C (1742°F) followed by slow cooling. For Grade 12 steel, ASTM 213 allows the finishing anneal for either hot finished or cold drawn tubes to be an isothermal anneal as follows: heat to 1200–1350°F (650ºC–730ºC) and furnace cool.
- Normalize and temper. Austenitize at about 950°C (1742°F) and cool in air. Under some ASTM codes, tempering is allowed at 580–720°C (1075–1325°F). European codes generally specify 1200–1325ºF (650–720ºC).
- Oil quench and temper. Austenitize at about 1000°C (1825°F), quench in oil, and temper at 570–705°C (1065–1300°F).

4.2.5 Microstructure

The final microstructure will depend on details of the composition and heat treatment. Component microstructures for tubes and pipes tend to be predominantly ferrite, with about 30% transformation product. The transformation product might be pearlite or bainite depending on details of the cooling rate. For fully annealed material, the relatively slow cooling rate usually results in a microstructure of ferrite and coarse pearlite. In normalized and tempered material, the faster cooling rates would normally produce a finer pearlite microstructure. However, if the pearlite lamellae are very fine, they will not be easily resolved using optical microscopy. Thus, in this case it is not easy to differentiate between transformation products. A typical normalized and tempered microstructure is shown in Figure 4-3.

It should be noted that although the final microstructure is determined by the cooling rate, the peak temperature and hold time used for the normalizing treatment will influence the austenite grain size. In general, this grain size can be controlled through a change in the temperatures used or through a change in the time a single temperature is held.

A variation in the peak temperature between 955°C and 1390°C (1750ºF and 2535ºF) for a low alloy piping steel results in an increase of the grain size from 20 µm to 200 µm. Moreover, for a given temperature, the grain size increases parabolically with time so that for any time-temperature combination, the grain size at a given time t is given by the equation

$$D_t^2 - D_o^2 = Const. \cdot e^{(-Q_c/RT)} \cdot t \qquad \textbf{Eq. 4-1 [5]}$$

where D_o and D_t are the initial and final grain size, T is the temperature, R is the gas constant, and Q_c is the activation energy.

Because casting involves solidification from the liquid, coarse austenite grain sizes are frequently developed. In components such as tubes and pipes that are worked during fabrication, working followed by reaustenitization will produce equiaxed microstructure. For these components, the thermal cycles associated with welding will introduce further microstructural modifications. Variations in peak temperature and cooling rate result in a range of different grain sizes and transformation microstructures within the weld metal and the HAZ. A micrograph of a typical Grade 11 low alloy steel weld is shown in Figure 4-4. The microstructure near the fusion line is shown (the weld metal is toward the

right side and the HAZ is toward the left). In the weld metal and HAZ, the cooling rate is relatively rapid so that the predominant microstructure is bainite. However, because of the differing thermal histories, a wide range of previous austenite grain sizes is present. Relatively slow cooling rates in the parent result in a predominantly ferritic microstructure; however, for parent sections that have been cooled rapidly, bainitic structures will prevail.

The heterogeneity of microstructures in a weld will typically result in a variation in properties. Normal subcritical post-weld heat treatment (PWHT) will reduce welding residual stresses and temper the microstructure. However, in some applications a full post-weld renormalization heat treatment is recommended. In this case, the weld and HAZ microstructures will be modified, with the formation of the final microstructure dependent on the normalization time and temperature and the subsequent cooling rate. A typical macrograph of a subcritical heat-treated weld is shown in Figure 4-5. This weld from a thick section main steam line is notable for at least two reasons. First, although the root area and initial fill passes have been produced using stringer beads, the majority of the weld has been produced with heavy weaving: this is not normally allowed. The second reason is that a creep crack developed during service in the HAZ.

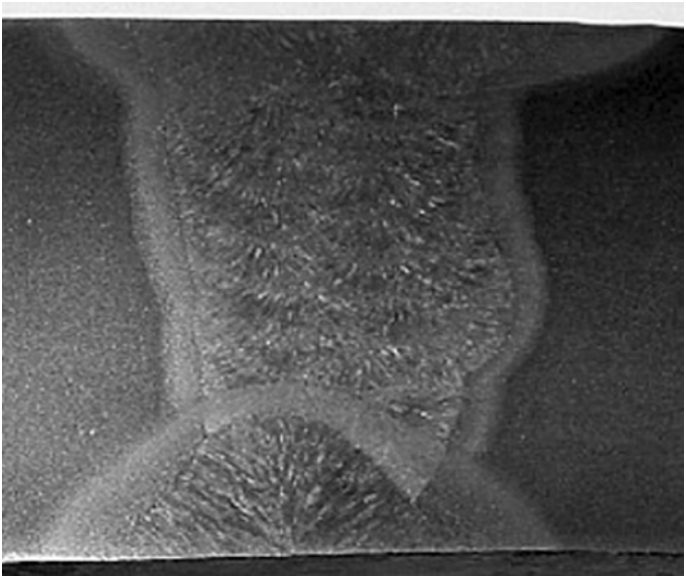

Figure 4-5
Macrosection Showing Grade 11 Weldment in Which the PWHT Involved Subcritical Heating [6]

4.2.6 Carbides in CrMo Low Alloy Steels

The type of precipitates formed will depend on the composition, the temperature history during fabrication, and the time and temperature of in-service exposure. Indeed, even though the preferred precipitates in steels are predominantly carbides (with nitrides and carbonitrides also present in many modern advanced steels), different carbide types will be present depending on service conditions. It is generally agreed [7] that the sequence of precipitation will be

$$M_3C \rightarrow M_3C + M_2C \rightarrow M_3C + M_2C + M_7C_3 \rightarrow M_2C + M_7C_3 + M_6C + M_{23}C_6$$

The carbide morphology in a pipe parent is shown in Figures 4-6a and 4-6b. Most of the carbides inside grains that were evenly dispersed were identified as M_2C and M_7C_3. The existence of M_7C_3 suggests that the regions shown in Figure 4-6b used to be bainite or pearlite before the service because M_7C_3 can be regarded as a transformation product of cementite.

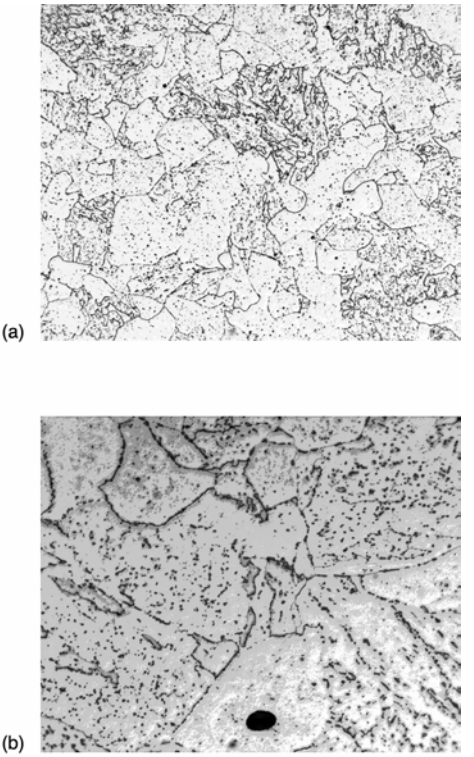

Figure 4-6
Optical Micrographs from a Section of T12 Superheater Tubing After Long-Term Service Showing the Precipitate Coarsening (Magnification for [a] is 200x and for [b] is 1000x)

In addition to the changes in carbide type, long-term service at elevated temperatures will result in growth of preferred carbides. This growth will be driven by the reduction of surface energy, which occurs when a large number of small precipitates are replaced by a smaller number of large precipitates [7]. These changes will occur by diffusion and, because diffusion along grain boundaries will tend to be faster than diffusion through the grains, there will be a tendency with increased aging for the largest precipitates to form at the boundaries. A typical electron micrograph showing the precipitate distribution in Grade 12 low alloy steel after long-term service at around 550ºC (1022ºF) is presented in Figure 4-7. This micrograph shows that the largest precipitates are present on the boundaries and that the growth of these precipitates has resulted in dissolution of neighboring precipitates. Thus, precipitate-free zones are developed so that the distribution of precipitate sizes is nonuniform. Because the strength of these alloys is largely a function of the ability of the precipitates to impede dislocations as growth takes place, there is a consistent reduction in strength.

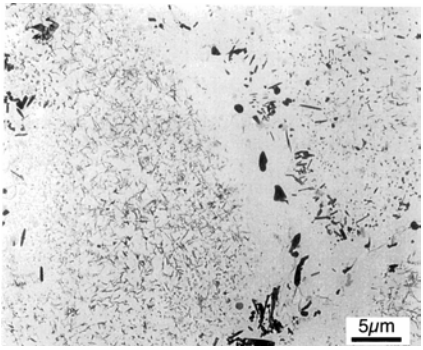

Figure 4-7
Detailed Electron Micrograph Showing the Typical Distribution of Carbides in Grade 12 Low Alloy Steel After Long-Term Service at Around 550ºC (1022ºF)

The trends in coarsening behavior are well established, and data of the type shown in Figure 4-8 have been compiled to monitor the effects of time-dependent aging. Of course, performing detailed electron microscopy is difficult, time consuming, and expensive. Thus, these changes are now normally inferred from optical microscopy or by monitoring hardness. Detailed optical evaluation of microstructural changes and the link to reductions in creep strength are shown in Figure 4-9. These trends are entirely consistent with the micrographs showing new, stage A structure in Figure 4-3 and the aged, stages E–F structure in Figure 4-6.

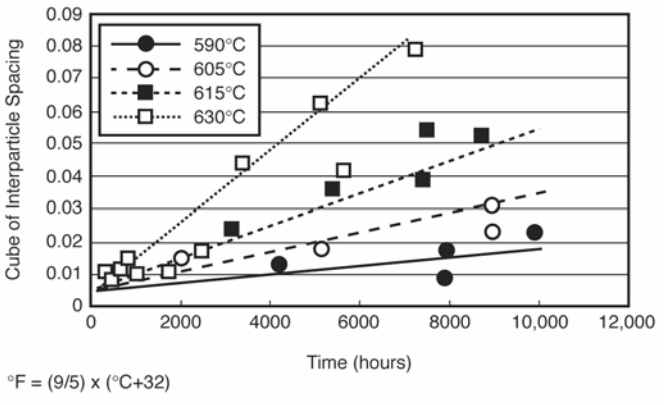

Figure 4-8
Detailed Measurements Showing the Coarsening of Carbides in Grade 12 Steel for Different Temperatures (As expected, the coarsening rate increases with exposure temperature.)

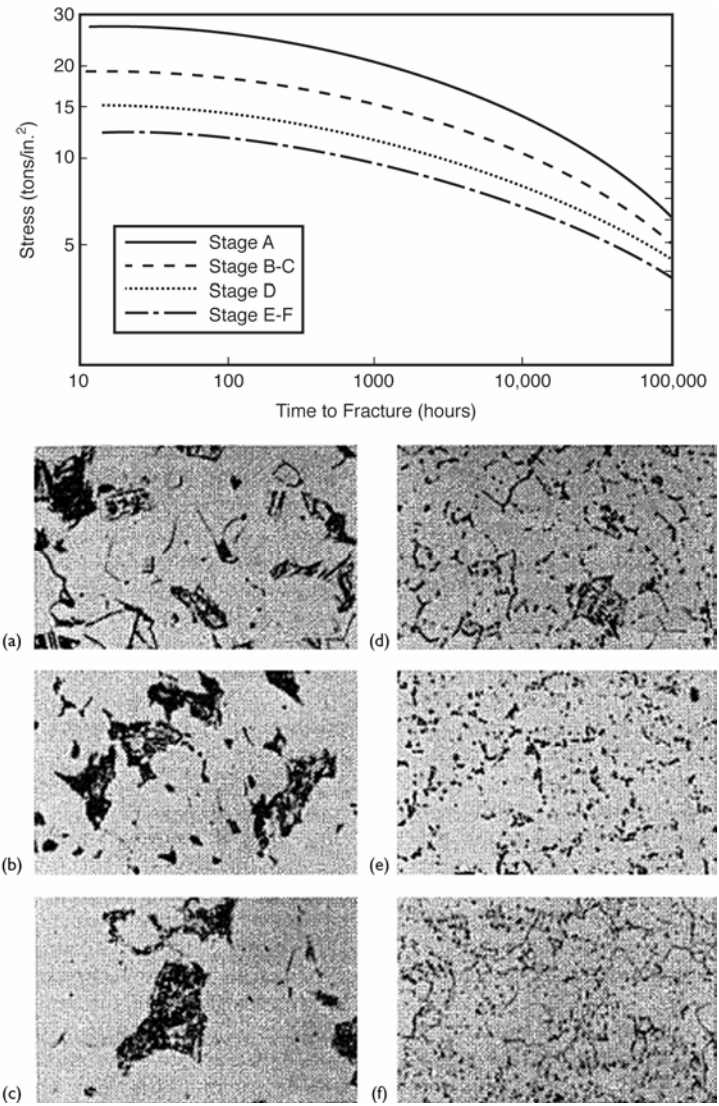

Figure 4-9
A Set of Optical Micrographs Illustrating the Microstructural Changes in 1CrMo Low Alloy Steel After Long-Term Service at Around 550ºC (1022ºF)

4.2.7 Hardness Changes

Microstructural changes are thus influenced by composition and temperature history. However, because the fundamental processes controlling microstructural development will be related to thermodynamics, the key process governing these changes will be diffusion. The generalized equation that relates the diffusion coefficient D and temperature T is as follows:

$$D = Const. \cdot e^{-\left(Q/RT\right)} \qquad \textbf{Eq. 4-2}$$

where Q is the activation energy of the process (in joules per mole [J mol^{-1}]) and R is the universal gas constant (8.31 J mol^{-1}K^{-1}). Processes that are controlled by diffusion will thus take place more rapidly as the temperature increases. Thus, it follows that

$$\frac{1}{t} = Const. \cdot e^{-\left(Q/RT\right)} \qquad \textbf{Eq. 4-3}$$

Taking logs and rearranging gives

$$T \cdot \{\log t + C\} = Q/2.3R \qquad \textbf{Eq. 4-4}$$

Thus, Q/2.3R is equivalent to the Hollomon-Jaffe Parameter for hardness changes [8]. Figure 4-10 illustrates the Hollomon-Jaffe relationship. (A similar derivation has been used for the Larson-Miller Parameter linking creep life to time and temperature [9].)

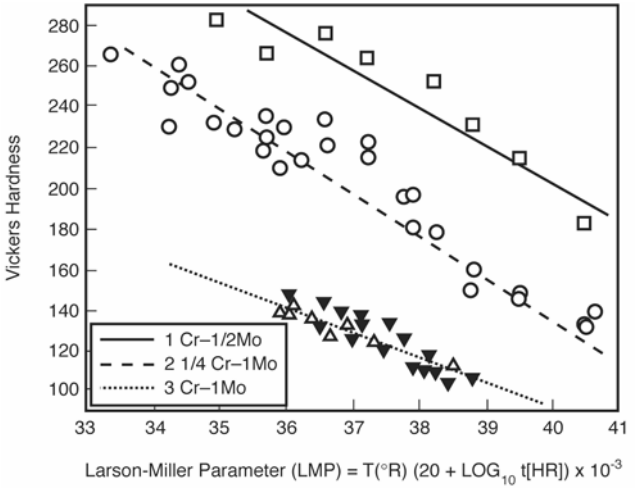

Figure 4-10
Reductions in Hardness in CrMo Steel as a Function of Time at Temperature Given by the Hollomon-Jaffe Parameter (see Equation 4-3)

These parameters have been widely used to allow development of descriptions linking time and temperature to particular properties or changes in properties. Specifically, the change in Vickers hardness has been monitored in laboratory evaluations of samples subject to controlled heat treatment schedules. The results obtained have allowed the following relationship to be developed:

$$H_v = 160.8 + 0.02793P - 1.9 \times 10^{-6}P^2$$

where *P* is calculated from the expression

$$P = T\,(11 + \log t)$$

and where *T* is in degrees Celsius and *t* is the time in hours.

The data obtained from these studies are shown in Figure 4-10. The 1CrMo data shown were taken from simulated HAZ microstructures that were aged for different times in the temperature range 1065–1200ºF (575–650ºC). The relationships shown in this section thus allow estimates to be made of equivalent operating temperature. Hardness readings taken after a known period of operation can be used to estimate an appropriate value of P because the time is known and an estimate of temperature will be

forthcoming. It should be noted that the temperature will be estimated as a single value, but because this estimate is based on diffusion processes, the estimate obtained will be relevant to an assessment of creep damage fraction. For high degrees of tempering, the hardness is relatively independent of initial structure. Therefore, the preceding relationships might be useful for the parent when long aging times or high service temperatures have been involved. It should be noted that work on 1CrMo steel has shown that accurate field hardness readings can be obtained only with a properly calibrated field instrument and with careful surface preparation—particularly for a parent that is predominantly ferrite. In most cases, a normally ground surface will not give accurate results unless high loads are used. Fine grinding or polishing is required to produce the necessary accuracy for most field applications.

5
PROPERTIES

5.1 Physical Properties

The following physical properties have been compiled from published information [10]:

- The *elastic modulus* of a material represents the relative stiffness of the material within the elastic range and can be determined from a stress-strain curve by calculating the ratio of stress to strain. Values are normally determined from tests performed in tension. The modulus of elasticity diminishes from 215 gigapascals (GPa) (30×10^6 pounds per square inch [psi]) at room temperature to 140 GPa (20×10^6 psi) at 760°C (1400°F).
- *Modulus of rigidity*, also known as the *shear modulus*, is the coefficient of elasticity for a shearing force.
- The *coefficient of linear thermal expansion* is the ratio of the change in length per degree kelvin (K) to the length at 273 K (32ºF). If l_0 is the length at 273 K and alpha is the coefficient of linear thermal expansion, the length at temperature T, l_t, is given by

  $$l_t = l_0(1 + \alpha T)$$

- The *thermal conductivity* (k) is the quantity of heat transmitted as the result of unit temperature gradient in unit time under steady conditions in a direction normal to a surface of unit area, when the heat transfer is dependent only on the temperature gradient.
- The *specific heat* (Cp) is the amount of heat measured in calories required to raise the temperature of one gram of a substance by 1ºC (34ºF). At room temperature, the value is 442 joules per kilogram (J/kg), with K increasing to 688 J/kg.K at 527ºC (981ºF).
- The *specific gravity* is the ratio of the density of a substance to the density of water.
- *Poisson's ratio* is the lateral contraction per unit breadth divided by the longitudinal extension per unit length. Poisson's ratio increases from 0.288 at room temperature to 0.336 at 760°C (1400°F).

Properties

- *Thermal diffusivity* is the constant in the heat conduction equation describing the rate at which heat is conducted through a material. It is linked to thermal conductivity, specific heat, and density (ρ) through the equation

$$K = l_{mfp} v = \frac{k}{\rho Cp}$$

Tables 5-1 and 5-2 present data tabulations, and Figures 5-1 through 5-5 show how selected properties vary with temperature.

Table 5-1
Typical Physical Properties at Room Temperature

	English Units	SI Units
Specific gravity	7.83	7.83
Density	0.2833 lb/in^3	7.83 g/cm^3
Thermal coefficient of expansion	7.3 x 10^{-6} °F (70–1000°F)	13.2 x 10^{-6} °C (21–538°C)
Modulus of elasticity at room temperature	29.7 psi x 106	215 GPa
Modulus of rigidity or shear modulus at room temperature	12.0 psi x 106	83 GPa
Specific heat	0.105 Btu/lb/°F (120–210°F) (see Note 1)	442 J/kg K at 23°C 688 J/kg K at 527°C 969 J/kg K at 727°C
Thermal conductivity	23 (Btu.ft/ft2.hr/ºF [70ºF])	39.5 (W/m-°C [21°C]) (See Note 2)
	22.2 (Btu.ft/ft2.hr/°F [600°F])	38.2 (W/m-°C [315°C])
Poisson's ratio at room temperature	0.288	0.288

Notes:

1 *Btu* stands for *British thermal unit(s)*.

2 *W* stands for *watt(s)*; *W/m* stands for *watt(s) per meter*.

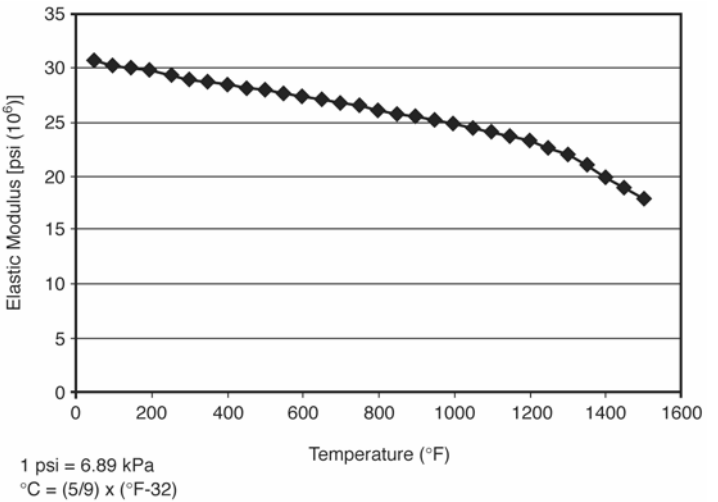

Figure 5-1
Variation in the Elastic Modulus with Temperature

Table 5-2
Variation in Selected Physical Properties with Temperature [10]

Temperature (°F) (see Note 1)	Thermal Conductivity (Btu/hr.ft.°F)	Thermal Diffusivity (ft2/hr)	Thermal Expansion [in./in./F($x10^{-6}$)]	Elastic Modulus [psi ($x10^{6}$)] (see Note 2)
50	21.2	0.417	5.35	30.5
100	21.5	0.409	5.53	30.2
150	21.8	0.400	5.71	29.9
200	21.9	0.391	5.89	29.6
250	22.0	0.382	6.09	29.3
300	22.0	0.373	6.26	29.0
350	22.0	0.365	6.43	28.8
400	21.9	0.356	6.61	28.5
450	21.8	0.347	6.77	28.2
500	21.7	0.337	6.91	27.9
550	21.5	0.327	7.06	27.6
600	21.3	0.320	7.17	27.3
650	21.0	0.310	7.30	27.0
700	20.8	0.299	7.41	26.7
750	20.5	0.288	7.50	26.4
800	20.2	0.278	7.59	26.1
850	20.0	0.268	7.66	25.8
900	19.7	0.258	7.73	25.5
950	19.4	0.248	7.80	25.2
1000	19.1	0.238	7.87	24.8
1050	18.8	0.227	7.94	24.4
1100	18.5	0.216	8.01	24.0
1150	18.2	0.204	8.08	23.6
1200	17.7	0.192	8.15	23.2
1250	17.2	0.178	8.22	22.6
1300	16.5	0.161	8.30	22.0
1350	15.3	0.138	8.37	21.0
1400	15.0	0.076	8.44	19.9
1450	14.9	0.130	8.51	18.9
1500	14.5	0.171	8.78	17.8

Notes:

1. ºC = (5/9) × (ºF-32)
2. 1 psi = 6.89 kPa

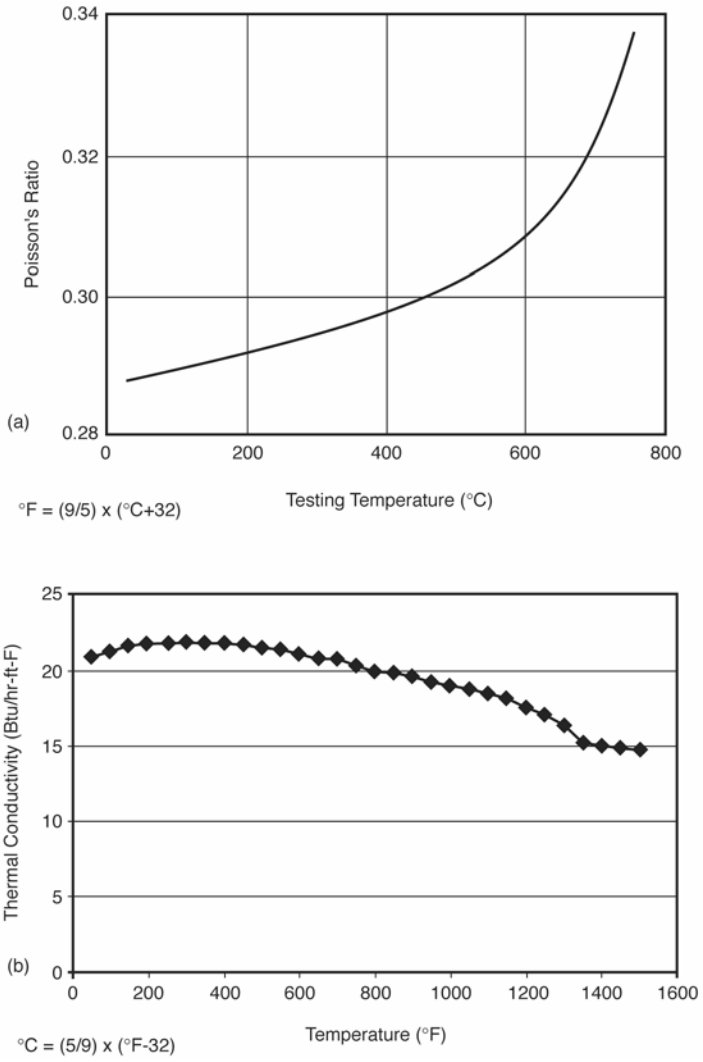

Figure 5-2
Variation in (a) Poisson's Ratio and (b) Thermal Conductivity with Temperature

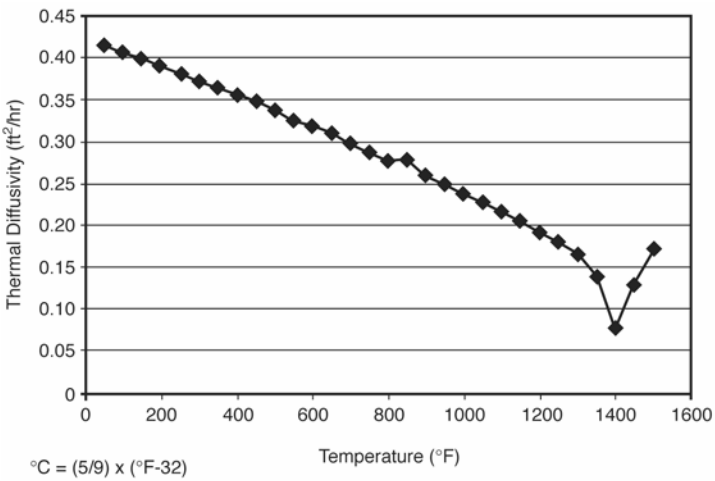

Figure 5-3
Variation in Thermal Diffusivity with Temperature

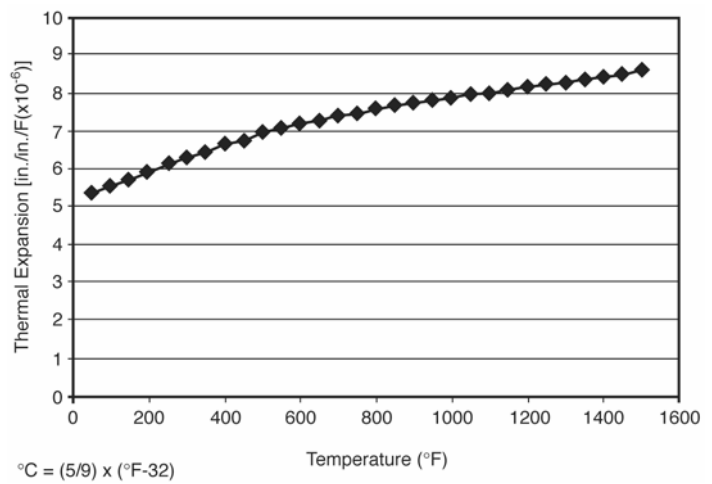

Figure 5-4
Variation in the Instantaneous Coefficient of Linear Thermal Expansion at the Indicated Temperatures

5.2 Tensile and Yield Strength

The effects of test temperature on the tensile and yield strengths as well as the average creep strength (0.01% in 1000 hours) and average 100,000-hour rupture strength of Grade 12 and 11 steels are illustrated in Figures 5-5 and 5-6, respectively.

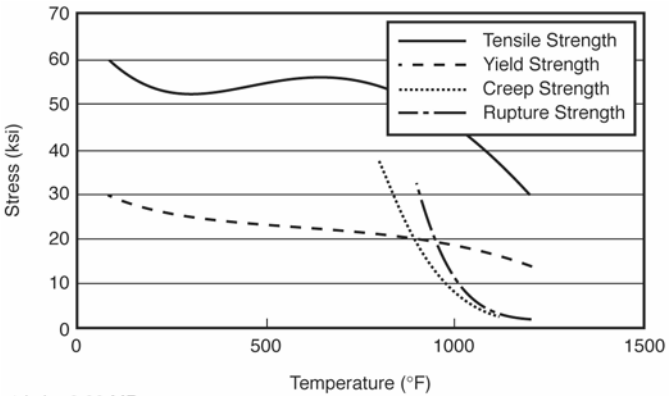

Figure 5-5
Variation in Yield Strength, Tensile Strength, Average Creep Strength, and Average 100,000 Hours Rupture Strength with Temperature for Grade 12 Material Heat-Treated in the Annealed Condition

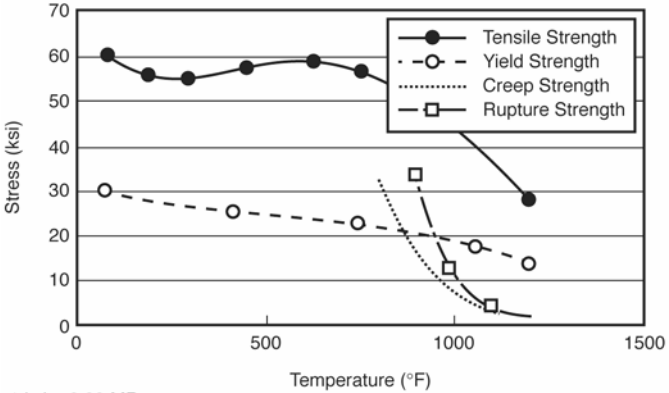

Figure 5-6
Variation in Yield Strength, Tensile Strength, Average Creep Strength, and Average 100,000 Hours Rupture Strength with Temperature for Grade 11 Material Heat-Treated in the Annealed Condition

5.3 Creep Properties

The creep behaviors of Grades 11 and 12 steels have been studied very thoroughly. The available parent metal data for these steels (that is, in the annealed or normalized and tempered condition) are summarized in three publications [11, 12, and 13]. In general, it is accepted that there is no significant difference in the creep behavior for the two alloys; therefore, the data sets are frequently taken together. A typical comparison of scatter bands for the two alloys is shown in Figure 5-7. General comments regarding the rupture strength and creep ductility of these steels follow:

- The stress-rupture strength generally increases linearly with room-temperature tensile strength up to about 565°C (1050°F) for times up to 10,000 hours.
- At a given strength level, tempered bainite results in higher creep strength than ferrite-pearlite aggregates for temperatures up to 565°C (1050°F) and times up to 100,000 hours. For higher temperatures and times, the ferrite-pearlite structure is the strongest.

- Rupture ductility generally decreases with rupture time, reaches a minimum, and then increases again. Test temperature, room-temperature tensile strength, austenitizing temperature, and impurity content increase the rate of decrease of ductility with time and cause the ductility minimum to occur at shorter time intervals.

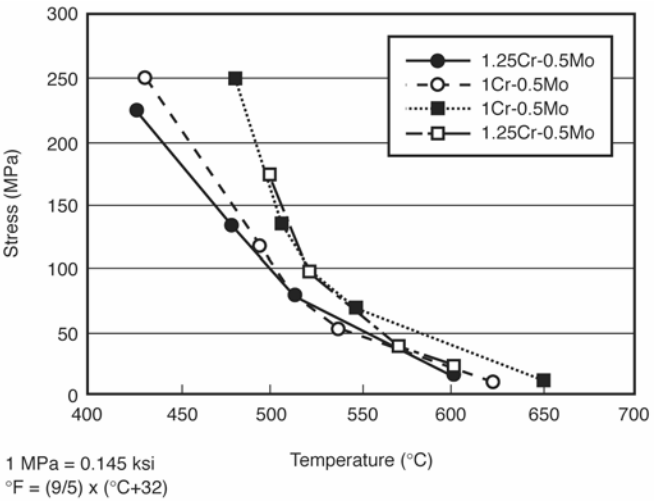

Figure 5-7
A Comparison of Creep Rupture Strengths in Grade 11 and Grade 12 Steels

The general creep behavior for annealed steels is shown in Figures 5-8a and 5-8b. The Larson-Miller Parameter can be estimated from the following equation:

$$LMP = 42896 - 5146(\log(\sigma)) - 2956(\log \sigma) \qquad \textbf{Eq. 5-1}$$

where σ is the stress, then

$$LMP = (T + 460)(20 + \log t) \qquad \textbf{Eq. 5-2}$$

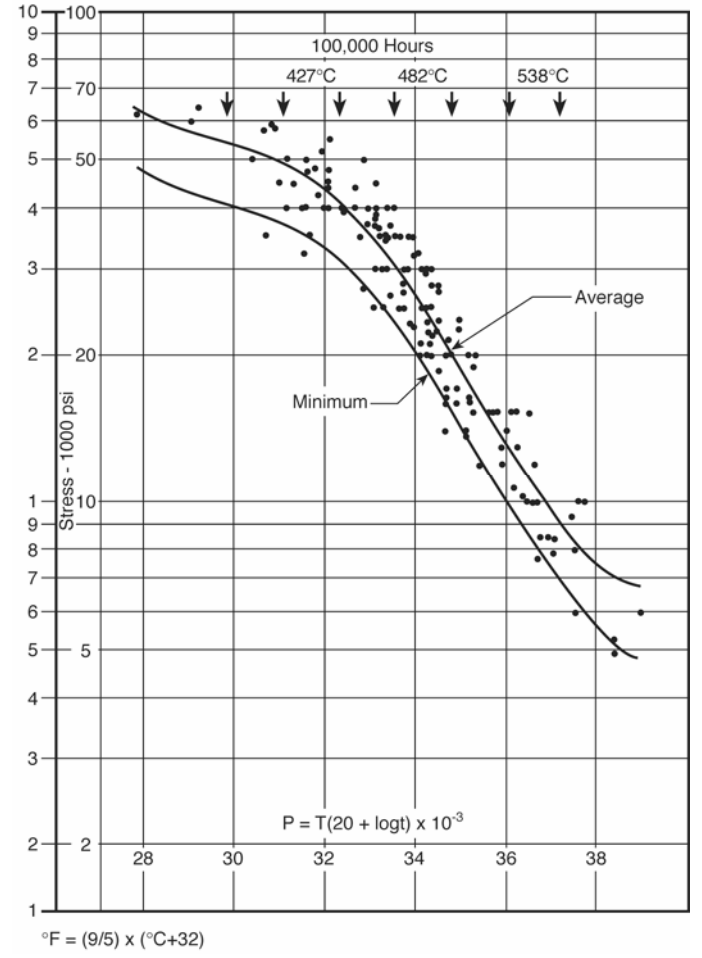

Figure 5-8a
Variation in the Larson-Miller Parameter with Applied Stress for Grade 12 Steel

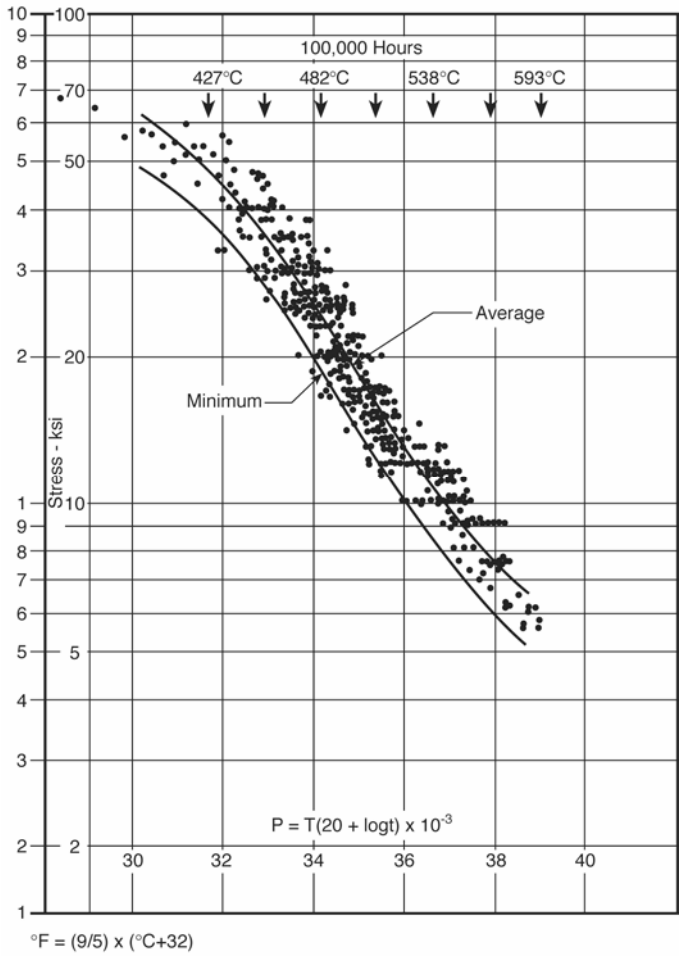

Figure 5-8b
Variation in the Larson-Miller Parameter with Applied Stress for Grade 11 Steel

Properties

For relatively short-term tests, the creep lives of welds are similar to those of the parent. However, in the longer term, the lives obtained for welds can fall below the minimum of the parent metal [13]. This reduced life might be the result of lower-than-expected properties for weld metals produced using the submerged arc process or damage developed in the HAZ at locations where the weld thermal cycles have resulted in excessive tempering. This form of damage is also known as *Type IV cracking*.

Because of the potential for welds to exhibit reduced life compared to the parent, a strength reduction factor should be applied. This reduction factor K increases the stress calculated for lifing purposes (σ) as

$$\sigma = \frac{\sigma_{comp}}{K} \qquad \text{Eq. 5-3}$$

When the Larson-Miller Parameter < 27810.6, the applicable value of K can be calculated using a parametric approach as follows:

$$LMP = (T + 460)(15 + \log tr)$$

and for Larson-Miller Parameters > 27810.6,

$$K_{weld} = -2.406 + (2.692 \times 10^{-4})LMP - 5.27610^{-9}(LMP)^2$$

5.3.1 Representations with Stress and Temperature

A number of alternative approaches for describing the variation of creep life with stress and temperature have been proposed. The results of a major European data evaluation program are shown in Figure 5-9. In this work, analysis has been performed for creep tests from a very wide range of sources, including test lives of more than 100,000 hours. The data analysis has allowed identification of stresses to give lives of 10,000, 100,000, 200,000, and 250,000 hours over a wide range of temperatures. The recommended average stress values are presented in Table 5-3.

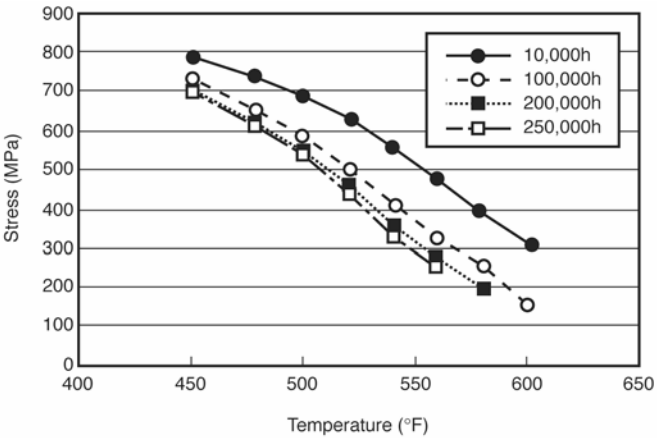

Figure 5-9
Combinations of Stress and Temperature Yielding a Range of Creep Lives

Table 5-3
Combinations of Stress and Temperature Yielding a Range of Creep Lives [14]

	Average Stress to Cause Rupture in Hours			
Temp.	**10,000 h**	**100,000 h**	**200,000 h**	**250,000 h**
°C	N/mm^2	N/mm^2	N/mm^2	N/mm^2
450	373	290	264	257
460	347	258	233	225
470	319	227	203	193
480	292	198	175	164
490	264	170	148	138
500	238	145	123	114
510	209	121	102	92
520	181	100	82	73
530	155	80	66	58
540	131	65	51	46
550	109	53	41	37
560	90	44	35	31
570	74	38	30	
580	60	31	25	
590	50	26		
600	41	20		

Similar results have been suggested based on evaluation of results from North American sources [11].

5.3.2 Creep Rupture

Long-term creep failures typically occur as the result of the nucleation, growth, and linking of grain boundary voids. Because these processes occur without significant macroscopic strain, such failures generally occur with low overall ductility. The fact that damage develops progressively

over time has permitted methods of component condition assessment to be developed. These approaches usually involve metallographic preparation of selected component locations followed by application of acetate replicas, which permits microscopic assessment. In the early stages of creep damage development, individual voids are observed (see examples in Figure 5-10). As further damage accumulates, the density of voids increases and the voids increase in size (see Figure 5-11). Eventually, the density of voids is sufficient for cracks to form. In thin components, crack formation will very rapidly lead to component failure. However, in thick section components, significant periods can be involved in crack growth.

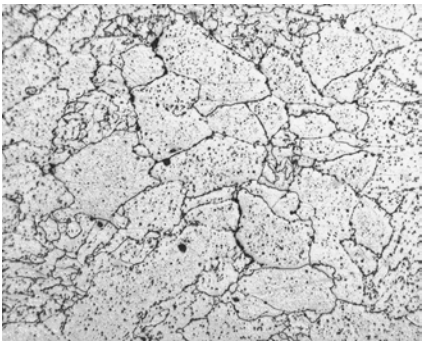

Figure 5-10
Creep Void Development in 1¼Cr¼Mo Steel Shown in an Optical Micrograph

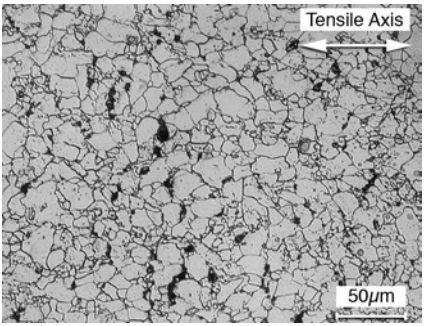

Figure 5-11
Alignment of Creep Voids Indicative of Damage Close to Microcrack Initiation

In many plant components, creep voids develop in the HAZ or weld metal. Typical micrographs showing early stages of damage are presented in Figures 5-12a and 5-12b.

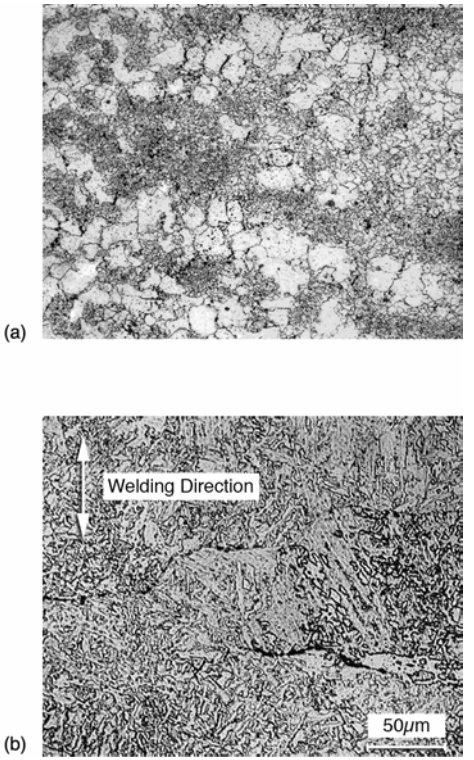

Figure 5-12
Creep Cavities Formed in the Intercritical (Type IV) Region of a Weld HAZ (a) and in the Weld Metal (b)

In view of the importance of creep development in the assessment of component condition, significant efforts have been made to relate the extent of creep microvoids to component life fraction. Initially, the methodology was semi-quantitative at best and considered only the general appearance of the voids. A desire to quantify the number of voids present on an individual grain boundary resulted in a damage classification system, with 1 used to indicate no damage and damaged boundaries classified as having D macrocracks (see Figure 5-13).

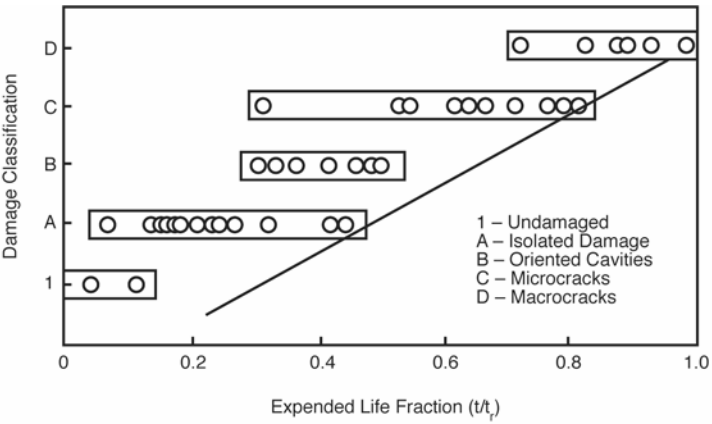

Figure 5-13
A Semi-Quantitative Relationship Between Creep Cavity Classification and Life Fraction [15]

Further efforts have been aimed at making the assessment more quantitative without requiring excessively time-consuming applications. One such approach [15] relates the number fraction of damaged grain boundaries A to creep life through the following expressions:

$$A = \frac{n_d}{\left(n_d + n_u\right)} \qquad \textbf{Eq. 5-4}$$

where n_d is the number of damaged boundaries and n_u is the number of undamaged boundaries, and

$$A = 0.517 \cdot \left(\frac{t}{t_r}\right) - 0.186 \qquad \textbf{Eq. 5-5}$$

The relationship developed from laboratory examination of specimens with known levels of creep damage is shown in Figure 5-14.

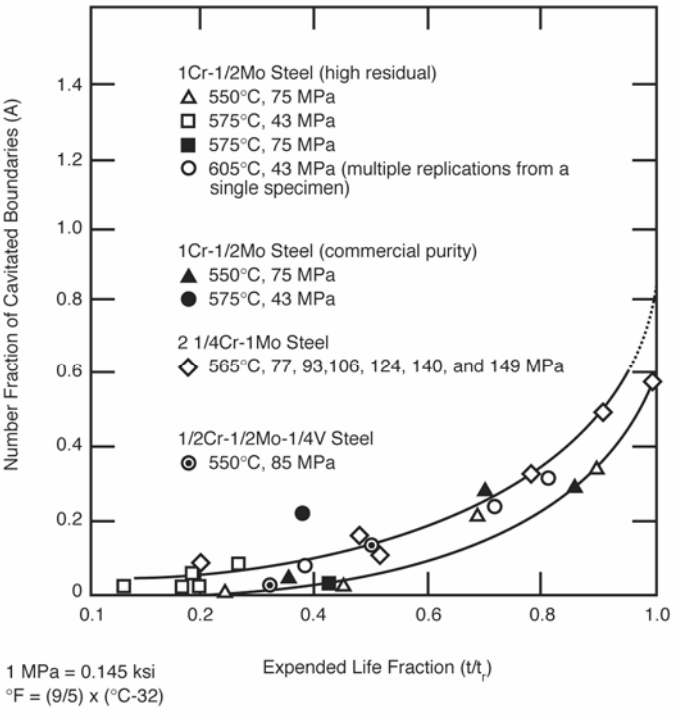

Figure 5-14
Relationship for Grade 12 Steel and Other Boiler Steels Showing the Number Fraction of Grain Boundaries with Creep Voids Present and Life Fraction [2]

In addition, approaches to assessing the level of life fraction consumed have been suggested based on consideration of both microstructural changes and the development of creep cavities. A typical sequence of damage development is given in Figure 5-15.

t/t_r	Microstructure
0	Ferrite plus bainite and/or pearlite M_3C and M_2C
0·2	Ferrite and partially disintegrated bainite/pearlite M_3C, $M_2C\uparrow$, and $M_{23}C_6\uparrow$
0·3–0·4	Ferrite and completely disintegrated bainite/pearlite $M_3C\downarrow$, $M_2C\downarrow$, $M_{23}C_6$, and $M_6C\uparrow$
0·4–0·6	Ferrite and coarse carbides $M_2C\downarrow$, $M_{23}C_6$, and M_6C Small number of irregularly spaced isolated cavities
0·6–0·8	As above, but more cavities Many cavities coalesced or about to do so
0·8–0·9	As above, but crack-like coalescence of cavities
0·9–1·0	Macroscopic cracking (removed from service)
* The observations of ferrite, bainite, pearlite, and cavitation are on an optical microscopic scale. The arrows indicate whether the phase concerned is increasing or decreasing with time.	

Figure 5-15
Description of Damage Development with Life Fraction for Grade 12 [2]

The fact that high temperature damage in these steels involves microstructural changes and the initiation and growth of creep cavities means that relationships between failure ductility and stress/temperature or rupture life can be complex. It is generally agreed that as rupture lives increase at one temperature, the failure ductility goes down as fracture becomes dominated by the initiation of grain boundary damage. At some point, the microstructural changes will make cavity development more difficult, and ductility begins to increase. Because the processes involved are dependent on diffusion, both time and temperature are important; for normal boiler temperatures, a minimum in creep rupture ductility can be expected (as an example, see Figure 5-16). At the lower temperature bound—below about 500ºC (932ºF)—there is insufficient thermal activation for the microstructure to age, and low ductility failures dominate. In contrast, at the upper temperature bound—above about 650ºC (1202ºF)—aging occurs so rapidly that low ductility grain boundary failures never take place. For the Grade 11 steel shown in Figure 5-17, ductility minima were clearly shown in tests at 593ºC and 620ºC (1099ºF and 1148ºF).

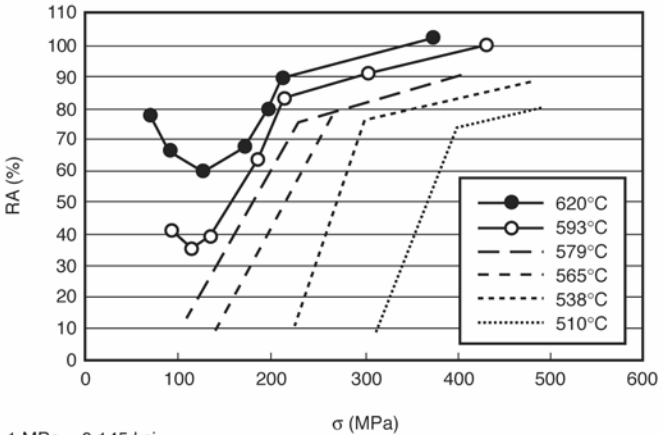

Figure 5-16
Variation in Reduction in Area at Fracture with Applied Stress for Creep Tests on Grade 11 Steel

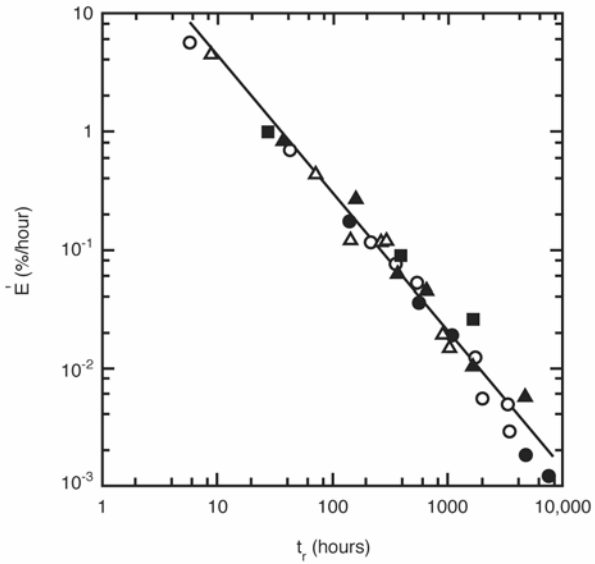

Figure 5-17
Relationship Between the Average Elongation Rate and Rupture Life for Creep Tests on Grade 11 Steel

In view of the importance of knowing failure ductility for in-service conditions, analysis has been carried out when good quality sets of results have been available over a range of stresses and temperatures. Evaluation of the data in Figure 5-16 has shown well-behaved relationships between the average creep elongation rate and the time to rupture. The results obtained (shown in Figure 5-17) indicate that for more than three orders of magnitude in rupture life, the data for Grade 11 steel could be described by the equation

$$(E\ tf)\ 1.18 = 66.8 \qquad \textbf{Eq. 5-6}$$

where E is the average elongation rate and t_f is the rupture life.

As an alternative to describing ductility in terms of stress and temperature, graphical representations showing ductility with time have been developed; Figure 5-18 provides an example. These representations show that under in-service conditions, the lowest ductility would be expected. Descriptions of this type provide an excellent aid in the selection of test conditions for laboratory programs because they facilitate identification of conditions that lead to low ductility failures.

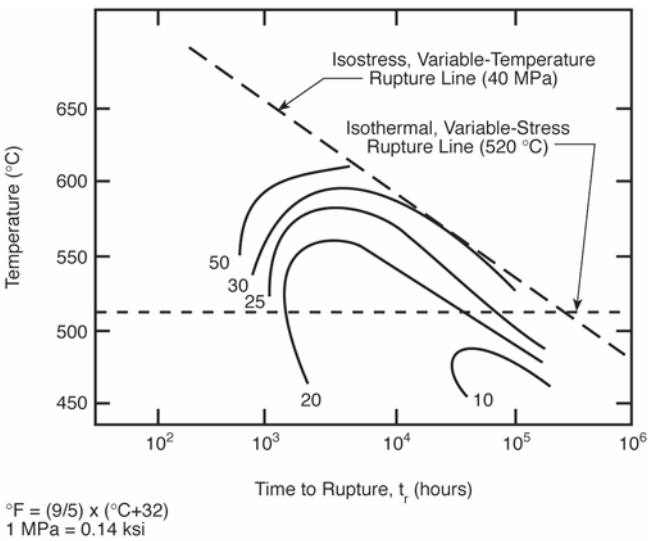

Figure 5-18
Isoductility Contours with Different Rupture Lives for Grade 11 Steel

5.4 Creep Crack Growth

Creep crack growth is usually described using the parameter C_t. This parameter can be calculated from the component geometry, loading conditions, and the crack dimensions [2]. A large number of experiments have been performed, and these demonstrate that creep crack growth can be described using the following equation:

$$da/dt = b\, C_t^{\,m} \qquad \text{Eq. 5-7}$$

A data set for Grade 11 steel at 1000ºF (538ºC) is shown in Figure 5-19. Relatively narrow bounds have been shown to describe creep crack growth behavior for base metal and welds in CrMo steels, as shown in Figure 5-20. The appropriate values of the constants are presented in Table 5-4.

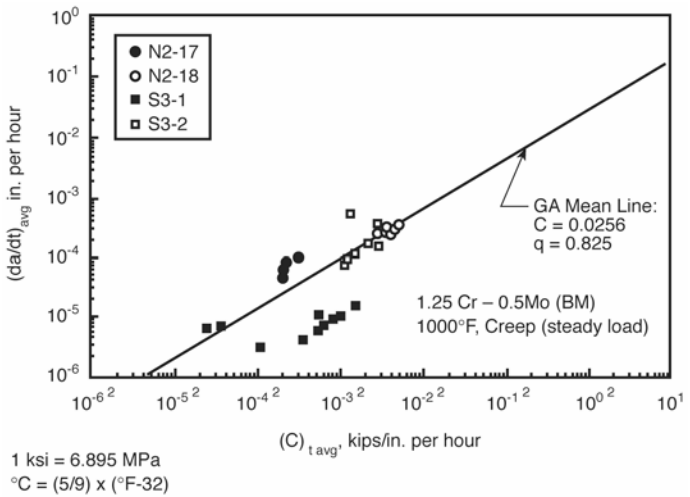

Figure 5-19
Average Creep Crack Growth Rate for Grade 11 Parent at 1000ºF [16]

Table 5-4
Summary of Creep Crack Growth Constants for Equation 5-7 [16]

Material	Values of the Constant b				Values of the Constant m	
	Upper Bound Line		Mean Line		Upper Bound	Mean
	BU	SI	BU	SI	BU	SI
Parent	0.094	0.0373	0.022	0.00874	0.805	0.805
Weld metal	0.131	0.102	0.017	0.0133	0.674	0.674
Fusion line	0.163	0.0692	0.073	0.031	0.792	0.792

Notes:

BU indicates units as follows: da/dt inches/h, C_t inch lb/inch2 h x1000.

SI indicates units as follows: da/dt mm/h; C_t kJ/m^2h.

Fusion line data exhibit fastest crack growth rate.

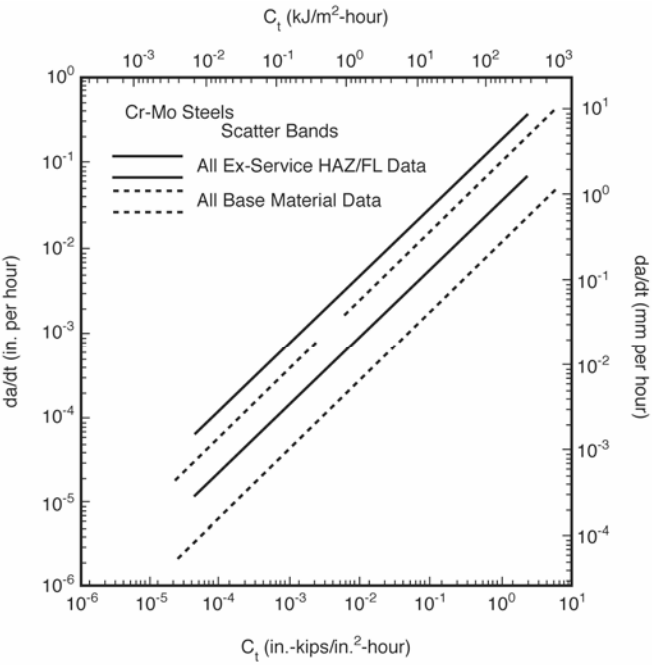

Figure 5-20
Comparison of Crack Growth Rate Scatter Bands for Ex-Service HAZ/Fusion Line Material and Base Material [16]

5.5 Fatigue Properties

Fatigue is the phenomenon of damage accumulation caused by cyclic or fluctuating stresses. During transient operation, such as startup, shutdown, and load changes, large thermal stress can be produced. The level of stress generated during a transient depends on several factors, including temperature range, temperature rate of change, and local component geometry. A severe temperature transient of even short duration can produce yielding. Thermal fatigue damage tends to occur at locations of thickness transitions and geometric stress concentrators at the interior surface of a high-temperature component. Tensile thermal stresses are

produced in a component during transient cooling, whereas compressive stresses are produced during transient heating. Therefore, cooling events need to be carefully controlled and monitored.

Significant transients can thus lead to problems associated with low cycle fatigue. These problems tend to occur in thick section components, such as casings, valve bodies, headers, and wyes and tees in piping. The stresses associated with low cycle fatigue are usually 60–80% of the ultimate tensile strength and are often associated with temperature and pressure changes to the component. The number of cycles to initiate and grow a crack to engineering size (0.05-in. [1.25-mm] deep or so) is usually on the order of several hundred to a few thousand. The number of cycles to failure depends on total strain range $\Delta\varepsilon\%$, as shown in Figure 5-21.

Mean lives can be estimated from the following equations [16]:

For $\Delta\varepsilon > 1.0726$,

$$N_f = 10^{(3.143 - 1.822\log(\Delta\varepsilon) + 0.2726(\log \Delta\varepsilon)2)} \quad \textbf{Eq. 5-8}$$

For $\Delta\varepsilon < 1.0726$,

$$N_f = 10^{(3.147 - 2.118\log(\Delta\varepsilon) + 4.601(\log \Delta\varepsilon)2)} \quad \textbf{Eq. 5-9}$$

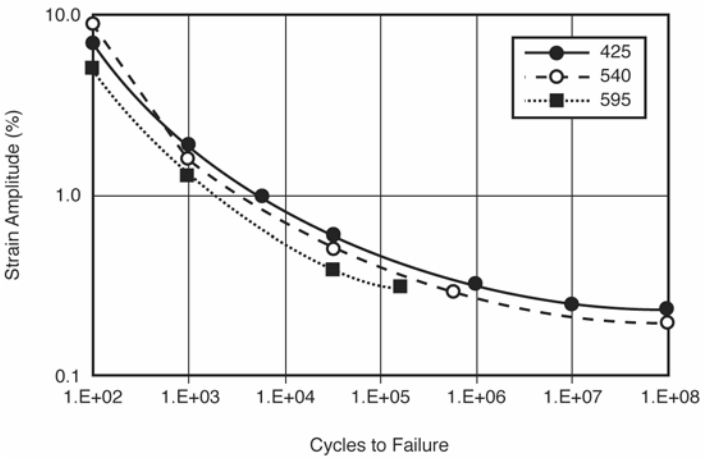

Figure 5-21
Variation in Cycles to Failure with Strain for High-Temperature Fatigue

5.5.1 Fatigue Crack Growth

Fatigue crack growth behavior (da/dN) is commonly described using the Paris Law. Namely:

$$\frac{\overrightarrow{da}}{dN} = C_{fat}(\Delta K)^n \qquad \textbf{Eq. 5-10}$$

As shown in Figure 5-22, the mean fatigue crack growth behavior for 1¼CrMo steel is described by the equation

$$da/dN = 5.34 \times 10^{-7} (\Delta K)^{1.083} \qquad \textbf{Eq. 5-11}$$

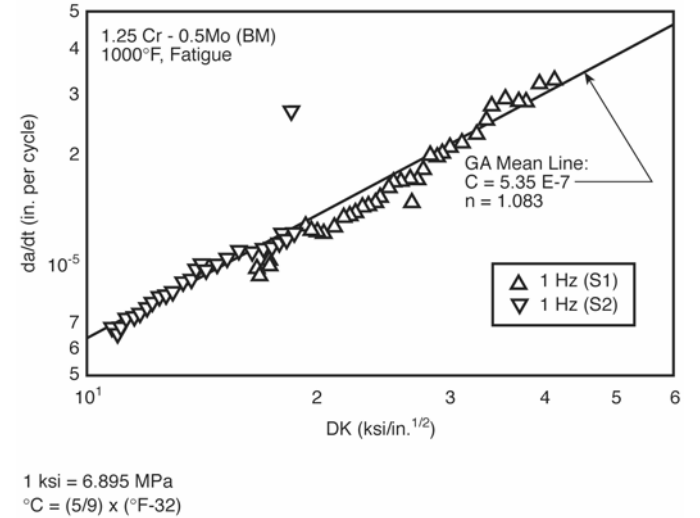

Figure 5-22
Fatigue Crack Growth Behavior

It should be noted that the fatigue crack growth rate has been shown to increase with increasing temperature. Thus, tests on both wrought and cast 1¼CrMo steel have shown that the crack growth rate increase was between two to four times on heating from room temperature to about 540–595ºC (1000–1100ºF).

5.6 Creep Fatigue Behavior

The introduction of a holding period at the peak strain of each high temperature cycle reduces fatigue life (for example, see Figure 5-23). From studies conducted on annealed 1¼CrMo steel in air [2], it is possible to conclude the following: 1) compressive hold periods are more damaging than tensile hold periods, and hold periods imposed on the tension side of the hysteresis loop are more damaging in terms of reduced cycle life than hold periods on the compression side; 2) linear damage summation of fatigue and creep damage lead to nonconservative estimates of component life.

The fact that the damage sums are less than 1 demonstrates an important creep-fatigue interaction. As shown in Figure 5-24, damage interactions are not adequately accounted for by the simple linear damage summation of fatigue and creep damage fractions. Indeed, when significant cycling involves hold times at high temperatures, the times to cracking are significantly reduced compared to linear damage predictions.

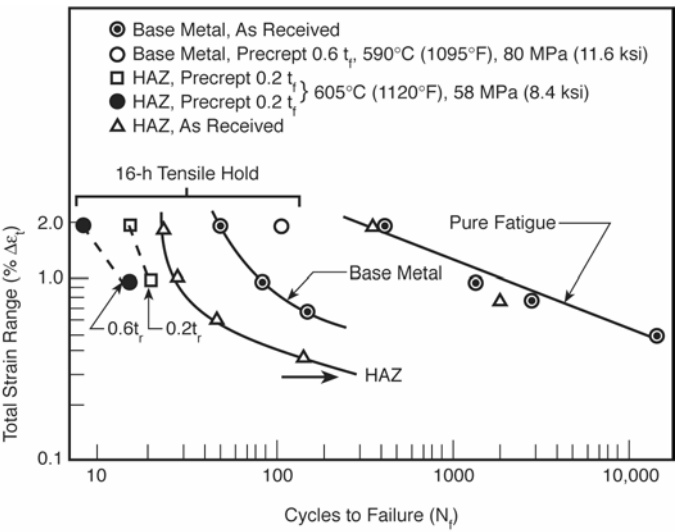

Figure 5-23
Test Results for Grade 11 Steel Showing That Holding at High Temperature Significantly Reduced the Number of Cycles to Failure [2]

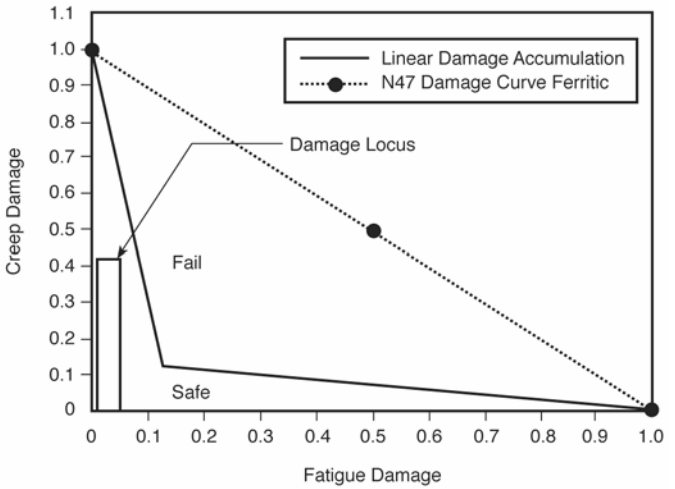

Figure 5-24
Creep Fatigue Interaction Diagram Showing That Linear Damage Estimates Significantly Overestimate Component Life

5.6.1 Creep Fatigue Crack Growth

For cyclic operation at elevated temperature (that is, at about 50% above the absolute melting point), the growth per cycle increases. The increase compared to room temperature is a factor of about 2 to 4 for ferritic steels and about 5 for austenitic steel (see Figure 5-25).

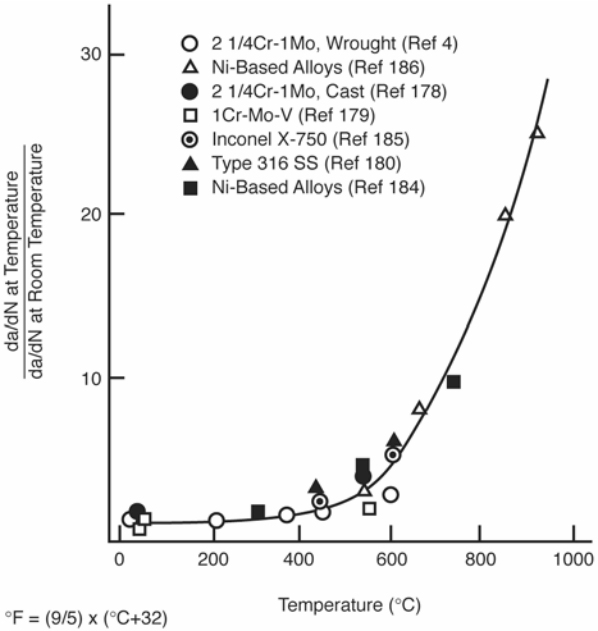

Figure 5-25
Effect of Increasing Temperature on the Cyclic Crack Growth Rate for a Range of Alloys Used in Elevated Temperature and Pressure Applications [2]

To account for the interactive effects, crack growth behavior must be described using terms for creep crack growth, fatigue crack growth, and an interaction term [10]. An appropriate equation is as follows:

$$\frac{da}{dN} = \underbrace{C'_1 \Delta K^m}_{\text{fatigue term}} + \underbrace{C_2 \Delta K^{2p} t_h^{1-p}}_{\text{interaction term}} + \underbrace{C'_3 C^{*p} t_h}_{\text{creep term}}$$

5.7 Toughness

Ferritic steels undergo a transition from brittle to ductile fracture. A number of approaches have been developed to assess this transition behavior (which is often described using the 50% fracture appearance transition temperature [FATT]), but the most common is the Charpy Impact Test. A large body of available FATT data has been compiled. Having determined the FATT, quantitative use of this information still requires that the FATT be converted to a fracture toughness parameter (K_{IC}). The EPRI report *Embrittlement of Components in Fossil Fueled Power Plants* [17] illustrates many published Charpy-fracture toughness correlations that can be used. Three correlations have been recommended in Annex J of the recent standard BS 7910 Guidance on Methods for Assessing the Acceptability of Flaws in Metallic Structures [18]. Two of these are used for materials on the lower shelf/transition of the ductile/brittle transition curve, and the third is recommended for upper shelf behavior.

For steels on the lower shelf and in the transition region, a simple lower bound estimate of toughness can be made from the Charpy energy measures at the temperature of interest. The appropriate expression is

$$K_{mat} = \frac{820\,(C_v)^{1/2} - 1420}{B^{1/4}} + 630 \qquad \textbf{Eq. 5-12}$$

where K_{mat} is a lower bound estimate of fracture toughness in $N/mm^{-3/2}$, B is the thickness (in mm) of the material for which an estimate of K_{mat} is required, and C_v is the Charpy energy (in J) for a 10-mm thick specimen tested at the minimum service temperature.

For ferritic steels using Charpy energy, the so-called *master curve approach* can be used to make a preliminary estimate of the fracture toughness of ferritic steels from Charpy energy. This is a valid approach—one based on a correlation between the 27-J transition temperature and the temperature at which a 25-mm thick fracture mechanics specimen shows a fracture toughness of 100MPa√m. The approach has been extensively validated for a range of parent steels that include Grades 11 and 12 steels (see Figure 5-26).

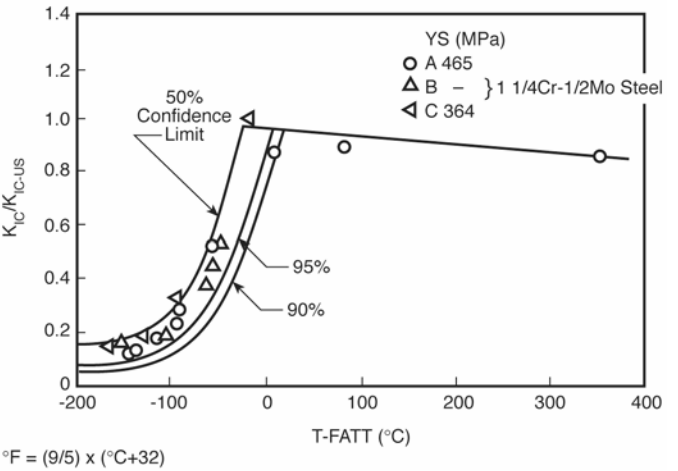

Figure 5-26
The Master Curve Approach Relating FATT with Fracture Toughness for Grade 11 Steel

In Figure 5-26, the ordinate is the fracture toughness normalized by the upper shelf fracture toughness K_{IC-US}, according to Equation 5-13 where

$$\frac{K_{IC-US}}{\sigma_{0.2}} = 0.6478\left(\frac{(CVN_{-US}}{\sigma_{0.2}} - 0.0098\right) \qquad \text{Eq. 5-13}$$

and where $CVN_{-US}(J)$ and $\sigma_{0.2}(MPa)$ are the impact energy and the 0.2% offset yield strength at the upper shelf temperature that is defined as the lowest temperature at which no evidence of brittle fracture is found. The narrow scatter of fracture toughness K_{IC}/K_{IC-US} is observed for the steels shown in Figure 5-26. Using these master curves, the fracture toughness transition curves of the materials can be easily obtained with successful results. The following are cases where the master curve approach overestimates K_{mat}:

- Charpy specimens exhibit unusual behavior, such as fracture path deviation.
- Splits are present on fracture surface of fracture toughness specimens due to crystallographic texture.

Properties

- Microstructure and properties vary through the section thickness, making it difficult to ensure that the Charpy specimen samples the same microstructure as that associated with initiation in the fracture toughness specimen.
- Mismatch-induced constraint can be a factor (highly over- or under-matched welds).
- Material is cold-worked.

The method takes into account the test temperature (T), the 27-J temperature (T_{27J}), the thickness of the specimen (B), and the desired probability of failure (P_f). Toughness at a given temperature is given by the equation

$$K_{mat} = 630 + [350 + 2435 \exp [0.019(T - T_{27J} - 3)]] (25/B)^{1/4} [\ln(1/1-P_f)]^{1/4} \quad \textbf{Eq. 5-14}$$

with units of K_{mat} in $Nmm^{-3/2}$, T and T_{27J} in °C, and B in mm. A value P_f = 0.05 (5%) is recommended for initial assessments. Note that this equation increases without limit as the temperature is increased, and it is important to take into account the onset of upper shelf behavior so that the upper shelf toughness is not overestimated.

This simple equation, also given in Annex J of BS 7910 [18], can be used to estimate the lower bound upper shelf toughness for cases in which the Charpy test results show 100% shear fracture:

$$K_{mat} = 17C_v + 1740 \quad \textbf{Eq. 5-15}$$

where C_V is the Charpy energy at the temperature of interest.

5.8 Aging Effects on Properties

It is apparent from the previous information regarding microstructural changes that the types of carbides present and the size of the carbides change with time at temperature. These changes usually lead to reductions in strength and hardness. In general, lower strength and hardness are considered to be associated with increases in ductility and fracture resistance or toughness. Although this trend is generally true for as-fabricated components, aging effects at elevated temperature can mean that strength and ductility are reduced. Two microstructural effects can lead to reductions in fracture resistance—the formation of networks of large carbides at grain boundaries and temper embrittlement.

These effects have been shown to influence a range of low alloy steels—including 2¼Cr1Mo steel—but neither of these phenomena has been proven to exhibit a major effect on Grades 11 and 12.

5.8.1 Carbide Embrittlement

The influence of carbides on the FATT has been evaluated in 2¼Cr1Mo steel using an alloy that is very low in trace elements. A step-cool heat treatment typical of the type used to evaluate temper embrittlement revealed that relatively low temperature exposure did not change FATT. In contrast, significant reductions in FATT were found after aging at 550ºC (1022ºF), 600ºC (1112ºF), and 625ºC (1157ºF). Considering both aging time and temperature, it was found that a reasonable description of the fracture behavior was obtained using the equation

$$\Delta FATT = A \times T (\log t + 8) + B \qquad \textbf{Eq. 5-16}$$

where A and B are constants. The change in FATT was directly related to the increase in the average size of the grain boundary carbides. No detailed results of this type are available for Grade 12 alloys.

5.8.2 Temper Embrittlement

Temper embrittlement is a major cause of degradation of toughness of ferritic steels [17]; components become candidates for retirement if they are severely embrittled because under these conditions, the critical crack size can become very small. The problem is encountered as a result of exposure in the temperature range of 345–540°C (650–1000ºF). Slow cooling following tempering or PWHT can lead to embrittlement, as can service exposure.

This problem has been identified in low alloy steels, stronger alloy steels, and stainless steels. It is traditionally a greater risk with components manufactured using older methodologies due to higher normalizing temperatures (these result in larger grain sizes), and when steel-making practices lead to higher levels of impurities, particularly impurities involving elements such as phosphorus, tin, antimony, and arsenic. Temper embrittlement occurs when these trace elements diffuse to grain boundaries. With respect to the behavior observed during Charpy Impact Testing, intergranular fracture rather than cleavage occurs in the brittle lower shelf region, and the transition from brittle to ductile takes place at a higher temperature; that is, there is an increase in FATT, which under extreme situations can be as much as 300ºC (572ºF).

Manganese and silicon in combination appear to affect the level of embrittlement when phosphorus is present. Thus, although it is clear that embrittlement can be noted in special alloys produced without manganese and silicon, in commercial alloys a systematic effect of greater embrittlement due to phosphorus at higher levels of the sum of manganese and silicon is identified. Indeed, there is evidence to suggest that there will be increased embrittlement with each of the elements individually because manganese is believed to reduce the grain boundary fracture strength and because silicon is believed to promote the segregation of phosphorus. A recent reevaluation of embrittlement data from a range of 2CrMo weld metals demonstrated that the variations in brittleness could be described on the basis of the negative effects of phosphorus, manganese, and silicon and the positive effect of molybdenum.

No systematic study is available for 1CrMo steels. However, some information has been evaluated from ex-service components. As shown in Figure 5-27, post-exposure measurements of FATT on reactor steels show some tendency for lower toughness with time at elevated temperature. However, there is significant scatter, and the trend is not clear.

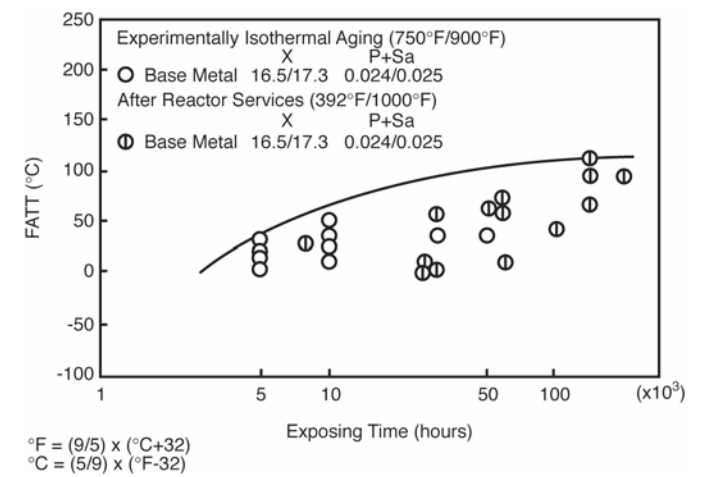

Figure 5-27
Measured Values of FATT for Different Times of Exposure at Elevated Temperature for 1CrMo Steels

The effect of trace elements on ductility has also been inferred from observations made during cause evaluations of cracked service components. Creep HAZ damage of the type shown in Figure 4-3 has been found in several different welded components. In the majority of cases, one HAZ is cracked with little or no physical evidence of distress observed at the other HAZ. This has been taken to indicate that the base alloy composition can reveal compositional information about the reasons for the greater susceptibility to cavity formation. For example, component weld was found to have developed creep microcracking and cavitation in the HAZ at one side of a weld. Chemical compositions of a flange, pipe, and weld metal are shown in Table 5-5. The parent material on the flange side, which is associated with the service-induced creep damage, contained higher tramp elements (such as phosphorus, tin, arsenic, and antimony) than a pipe parent that shows no creep damage.

Table 5-5
Chemical Compositions of Materials (by Percentage Weight)

	Flange	Weld Metal	Pipe
Carbon	0.12	0.066	0.10
Silicon	0.43	0.43	0.65
Manganese	0.51	0.61	0.47
Chromium	1.31	1.37	1.21
Molybdenum	0.54	0.57	0.45
Titanium	<0.001	0.009	0.002
Vanadium	0.005	0.008	0.002
Niobium	<0.002	<0.002	<0.002
Sulfur	0.015	0.009	0.004
Phosphorus	0.015	0.009	0.012
Tin	0.023	0.012	0.012
Arsenic	0.029	0.019	0.012
Antimony	0.003	0.01	0.001
Copper	0.11	0.092	<0.05
Creep Embrittlement Factor	0.192	0.180	0.056

Properties

Takamatsu et al. [19] correlated the impurity contents using the following factor with creep ductility at the coarse grain zone (CGZ) for Grade 11 steel. This factor, termed *creep embrittlement factor* (C.E.F.), was originally proposed by King to assess the susceptibility to stress relief cracking for ½Cr½Mo¼V steel [17]. The C.E.F. is calculated as follows:

$$C.E.F. = P+3.57Sn+8.16Sb+2.43As \quad \textbf{Eq. 5-17}$$

Though threshold value to assess the likeliness of premature cracking at the CGZ has not been derived, values of C.E.F. for the cracked reactors made from Grade 11 steel found in relevant papers were higher than 0.15. A simple direct correlation of this factor with susceptibility for damage is complicated because in addition to differences in composition, there might also be variations in microstructure. In the present case, the damaged component was a forged flange that showed a predominantly bainitic transformation product. On the other hand, the microstructure of the pipe parent was ferrite-pearlite. This difference in microstructure might have been a contributing factor. Nevertheless, evaluation of information regarding local microstructure and composition to allow the C.E.F. to assess increased susceptibility to cracking has been and will continue to be used in component assessment.

6
OXIDATION RESISTANCE

6.1 Scale Formation

Oxidation of boiler tubing in fossil boilers occurs naturally at all temperatures [20]. Under normal conditions, these scales are continuous and protective. Table 6-1 gives guidelines on the maximum temperature for typical boiler steels in steam service according to applicable codes and manufacturers.

Table 6-1
Maximum Tube Metal Temperatures [21]

ASME Specification	ASME °F/°C	Babcock & Wilcox °F/°C	ALSTOM °F/°C	Riley °F/°C
SA-213 T11	1200/649	1050/566	1025/552	1025/552

These scales will grow at a rate dependent on the temperature (see Figure 6-1), and this has permitted measurements of scale thickness to be used as an aid to tube life estimation, particularly in the superheater and reheater tube sections. Under non-ideal conditions, laminations can occur in the normally adherent oxide scales (see Figure 6-2). When the scale becomes excessively thick, the heat transfer from the metal to the superheated steam becomes inhibited. As a guide, 0.001 in. (0.025 mm) of scale thickness will raise the tube temperature by 1–2ºF (0.5–1ºC). Thus, oxides of 0.020–0.040 in. (0.5–1 mm) can raise the operating temperature by 40–80ºF (22–44ºC). Temperature increases of this level will significantly reduce tube life. It should therefore be appreciated that excessive scale formation is a contributing factor to long-term overheat failures.

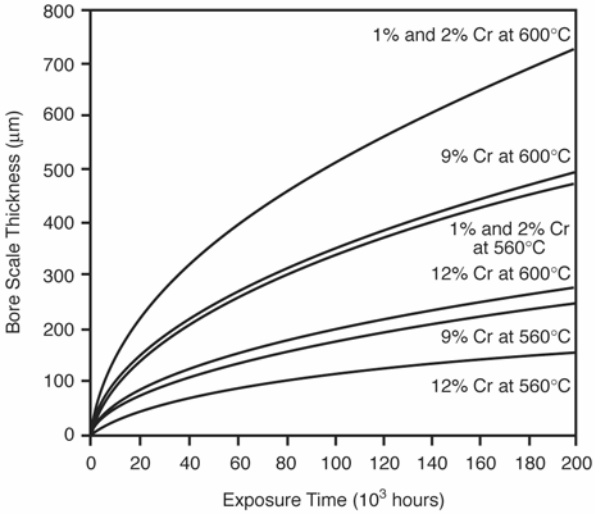

Figure 6-1
Data Showing How Steam-Side Scale Growth Varies with Temperature for Boiler Alloys with Different Compositions of Cr [22]

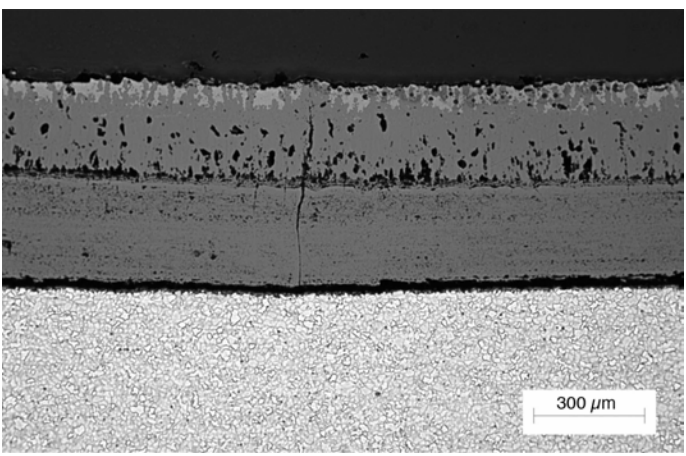

Figure 6-2
Typical Micrograph Showing Laminated Steam-Side Scale Developed on a CrMo Tube

6.2 Growth of Laminated Scales

Only a very brief description of laminated scales will be given here: full details of the metallography and mechanisms of formation are available elsewhere [20, 22]. A typical example of a laminated scale is shown in Figure 6-2. These scales consist of pairs of layers of magnetite and iron-chrome spinel. The magnetite layer at the steam/scale interface is considerably thicker than any of the other layers and is paired with a spinel layer that might be less than half its thickness. The component layers of the remaining pairs are of roughly equal thickness, and although the thickness of the pairs was found to vary from < ~1 μm to ~50 μm, no consistent trend in this variation across the scales was observed. Metallographic examination of the scales indicated that growth of the oxide laminations takes place at the metal interface and immediately adjacent to it underneath the oxide layers already formed. Thus, the mechanism of growth in the pairs of layers is probably similar to that of the duplex oxide scales formed on low Cr steels in several environments.

Growth of the magnetite layer takes place through the outward diffusion of iron through the oxide scale with the formation of new oxide at the outer magnetite surface. In laminated scales, this growth will be at the interface between the bottom of the spinel layer of the previous pair of laminations and the top of the magnetite layer of the currently growing pair. The spinel layer in a pair of laminations grows by the inward diffusion of oxygen to the metal/scale interface and effectively fills the volume left behind by the iron that has formed the outer layer. The extra thickness of the outermost magnetite layer over the spinel layer with which it is paired probably arises through the continued diffusion of some iron to the steam/scale interface during the growth of the laminations.

6.3 Oxidation Rate of 1¼CrMo Steels in Steam

The scale formed during steam oxidation of low alloy steels has three distinct regions when cross-sectioned: a thick, compact outer layer; a subscale region consisting of extensive internal oxide precipitate formation mostly along the grain boundaries; and a thin layer between the outer layer and the subscale. It is claimed that a critical balance of the selectively oxidized metal, the oxidant species, and the growth rate of the external scale governs the extent of the internal oxide precipitation and subscale formation [20].

There is a distinct difference in the structure and morphology of the oxide scales formed under dry air oxidation versus those formed under steam oxidation. A recent study in which specimens were oxidized at 600°C (1112°F) in a mixture of steam and nitrogen reported that the scales developed during steam oxidation on CrMo steel consisted of faceted oxide grains, whereas the morphology of the air-oxidized specimens was reported to be featureless. It was noted that the structure of the scales on the steam-oxidized specimens were free of surface pores and that the oxide grains were closely compacted to each other. This is distinctly different from the porous outer scales observed under air oxidation.

General observations have indicated that the oxide scale, which forms on the steam side surface of CrMo steel boiler tubes, generally consists of a multi-layered scale. The composition of the scales is predominantly magnetite and wustite (Fe_3O_4 and FeO, respectively); however, there is also evidence in X-ray patterns of the presence of an iron Cr spinel oxide ($FeCr_2O_4$). Specific observations have indicated that at temperatures below 560°C (1040°F), a scale consisting of magnetite and haematite (Fe_2O_3) is found. At higher temperatures, an additional inner layer of wustite can be present, and a spinel oxide (such as FeO_4, CrO_4, or MoO_4) will form as the oxide grows inward across the tube wall [20].

The current understanding is that the wustite formation temperature is approximately constant at 560°C (1040°F), independent of the alloy in question. This suggests that at temperatures below 600°C (1112°F), Grade T22 obeys a parabolic law, which indicates that at these temperatures the materials are self-protecting. Thus, the behavior is described by the simple expression

$$\text{Mass change} = k\, t^{1/2} \qquad \textbf{Eq. 6-1}$$

However, at high temperatures, the scale becomes non-protective, and the kinetics approach linear behavior. Care must be taken in evaluating oxidation data from experiments related to in-service behavior because the rates of oxidation differ with the environment. Generally, the oxidation rate in flowing steam is about twice that in a mixture of steam and carrier gas. Comparing behavior for Grade 11 and 12 alloys, it should be noted that because an increase in silicon content reduces the steam-side scale formation, steam-side scale formation in Grade 11 would be expected to be less than in Grade 12.

It is possible to describe the amount of metal consumed during steam oxidation of a number of low alloy steels by an equation of the following type:

$$X_o = K_O \exp(-A_O/T)\, t^{1/2} = W_o/2 \qquad \textbf{Eq. 6-2}$$

where X_o is the thickness of metal consumed (in μm), W_o is the thickness of the scale (assuming a Pilling-Bedworth ratio of ~2 for duplex scale), t is the duration of oxidation (in kilo hours), T is the absolute temperature (in K), and A_o and K_o are constants. A detailed review of available data for the oxidation rate of low alloy steels in steam has been performed [21, 22], and the results are summarized in Figure 6-3.

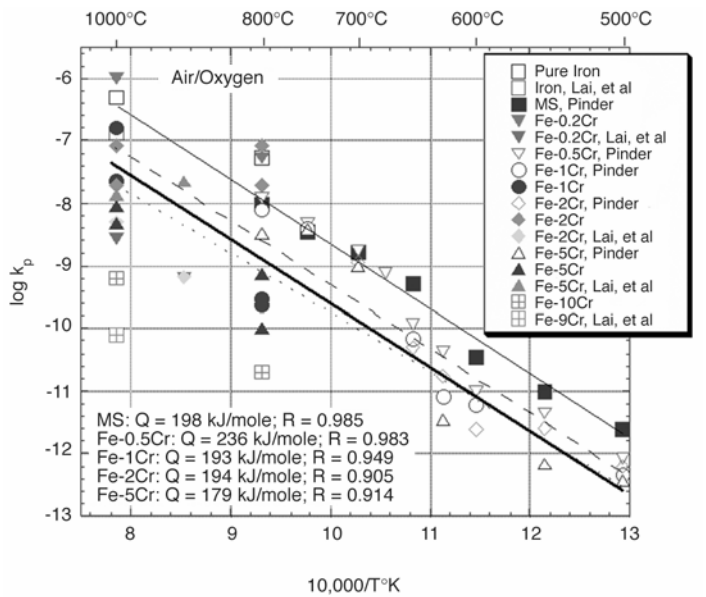

Figure 6-3
Summary of the Oxide Growth Constant for Iron, Carbon, and Alloy Steels [22]

When a new pair of layers forms at the metal/scale interface, the scale growth rate returns to the value at zero time. Growth then continues according to Equation 6-1 (parabolic) until a new pair of layers forms, at

which time growth returns to the value at zero time. The overall growth rate will be given by the sum of a series of parabolae, and when the time between successive laminations is small compared with the total duration of oxidation, growth will appear to be linear. The factors that determine the initiation of laminated scale growth or the point at which new laminations form once this growth mode is established are being intensively investigated but are not yet fully understood. However, for the purposes of calculating the growth rates of laminated scales, it is assumed that a new lamination is formed after the currently growing lamination has reached a given thickness. An advantage of this is that the rate of laminating can be directly correlated with measurements of the thicknesses and the number of laminations from micrographs of the scales.

If the laminations have a thickness (the inner plus outer layer) of L μm, according to Equation 6-1, the time required growing one lamination t' will be given by

$$t' = L^2/ [2K_O \exp (-Ao/T)]^2 \quad \textbf{Eq. 6-3}$$

When the scale grows at a paralinear rate, the thickness W_o after time t will be given by

$$W_o = 4/ L [K_o \exp(-Ao/T]^2 t \quad \textbf{Eq. 6-4}$$

Linear rates of oxide growth calculated when new laminations form every 50 μm, 100 μm, and 200 μm of scale thickness show much higher growth rates compared with parabolic oxidation. Evaluation shows that the description of the growth of laminated scales in terms of a linear rate law is a good approximation for plant oxidation times (thousand of hours) and lamination thicknesses <100 μm.

6.4 Life Assessment by Oxide Thickness Measurements

Scale thickness measurements are widely used in life assessments of steam generator tubes in fossil fuel power plants. In a typical steam generator tube bank, although the average steam temperature might be within design limits, the local steam temperature in some of the superheater and reheater tubing can be as much as 100ºC (212ºF) higher than the bulk temperature. Exposure to this increased temperature can cause a rapid loss of tube life. A nondestructive measurement of the oxide scale thickness across the tube bank suggests whether a given tube has

developed an excessive scale thickness. An above-average scale thickness is taken as indicative of an excessively high temperature, which could deteriorate the remaining life of the particular tube and necessitate replacement of the tube bank. To correlate the thickness of the in-service oxide scale with the temperature history of a component, scale growth rate data are generated over a range of temperatures. For the purpose of life assessment, the power-industry-based research groups have also generated long-term scale growth data over an industrially relevant range of temperatures.

6.4.1 Metallographic Measurement of Steam-Side Scales

A representative macrograph of one tube section is shown in Figure 6-4. As is normal for many superheater and reheater tubes, the hottest regions occur where the tube has maximum exposure to the hot gases. These locations are typically at the 10 o'clock and 2 o'clock locations. In Figure 6-4, these hot locations have been associated with significant time-dependent wall loss. Moreover, because these locations will have been operating at significantly higher temperatures than the rest of the tube, the steam-side scale will be significantly thicker here. This observation illustrates the need to ensure that measurements of steam-side scale taken to aid tube life assessment are taken at the hottest locations. It is not unusual for the variation in thickness around the tube to be up to a factor of 2. Clearly, measurement away from the thickest location will underestimate the operating temperature and lead to nonconservative estimates of performance. Generally, the areas of thickest scale coincided with the thinnest tube wall section and thickest fireside scale. However, appropriate detail should be used when taking measurements to ensure that accurate data are obtained.

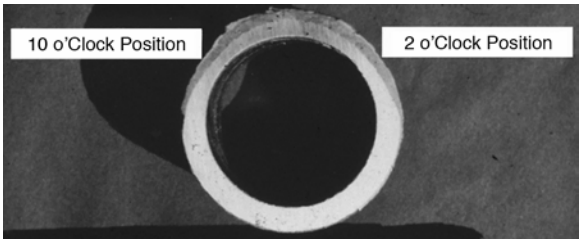

Figure 6-4
Typical Ex-Service Tube Showing the Buildup of Scale and Wall Loss at the 10 O'Clock and 2 O'Clock Positions

6.4.2 Ultrasonic Measurement of Oxide Scales

Nondestructive ultrasonic techniques are available for obtaining wall thickness and internal oxide thickness measurements from in-service tubing. As shown in Figure 6-4, there is frequently synergy between the highest operating temperatures and wall loss so that practical methods for determining oxide scale from tubing benefit from simultaneous measurements of wall thickness. The most recent of these techniques uses computer-based digital technology so that measurements are both accurate and rapid. This high efficiency allows greatly increased numbers of tubes to be measured, making it possible to develop detailed maps of oxide thickness. Using the established relationships between scale development with time/temperature, these data provide important input to tube life calculations. The results of these measurements thus allow estimates of tube remaining life.

7
FABRICATION ISSUES

In the United States, 1¼Cr1Mo low alloy steel is normally manufactured in an electric furnace. In Japan, basic oxygen processes are used. For certain critical applications, vacuum arc remelting or electroslag remelting is appropriate.

7.1 Workability and Forming

It is important to distinguish between the production route for the various material specifications for wrought products (such as tubes, pipes, forgings, and plates) used by the material producer and the subsequent fabrication practices used to convert these products into finished shapes used by the manufacturer. In general, material producers use hot working processes to take advantage of the workability arising from lower strength at high temperature. Thus, high-temperature operations for plate rolling, forging, or tube/pipe extrusion begin at very high temperatures—typically 2000–2400°F (1095–1315°C)—and finish substantially above the AR_3 temperature (see Section 4.2.1) of 1550°F (821°C) for Grade 11 steel. This ensures that all the high-deformation processes are performed with the material in the austenite phase. Following this initial hot forming, many products are final-sized at lower temperatures, followed by an eventual final heat treatment (normalize, normalize and temper, anneal, isothermal anneal) to meet the product specification.

The focus of the remainder of this section will be the working and forming operations performed by the component manufacturer (in other words, fabrication). The critical transformation temperatures, which were discussed in Section 4.2.1, play a key role during fabrication. In particular, the *on-heating* transformation temperatures, AC_1 and AC_3, were previously discussed as well as the *on-cooling* transformation temperatures, AR_3 and AR_1. These critical temperatures are sensitive to composition and to heating and cooling rate; caution is advised in trusting published values as being absolute. Nevertheless, general guidance is necessary to set limits related to fabrication. Because transformation is a non-equilibrium process, the on-heating transformation temperatures occur above the equilibrium values for A_1 and A_3, and the on-cooling transformation temperatures occur below the equilibrium temperatures.

Fabrication Issues

For ferritic steel tubes, ASME Section I gives no guidance relative to heat treatments that are appropriate following fabrication involving hot or cold forming. Silence on this subject should not be interpreted to mean that it is not an important issue. Indeed, an activity is underway in Section I to prepare appropriate rules for ferritic steels to parallel the rules in PG-19 for austenitic stainless steels. But at the moment, the issue of post-forming heat treatment is a contractual matter between the manufacturer and customer, and all of the boiler original equipment manufacturers (OEMs) have internal practices covering the usual construction materials.

The subject of post-forming heat treatments is complex. The practices that have evolved have been based largely on service experience with limited systematic laboratory studies. Some of the relevant variables believed to be influential in determining the need for post-forming heat treatment for ferritic steels follow:

- Generic material type with susceptibility increasing with alloy content—that is, increasing hardenability.
- Specific chemical composition within the broader generic material specification.
- Deoxidation practice in which there is an interplay between the deoxidant and other elements. For example, if aluminum is used for deoxidation, the Al/N ratio is likely to be important.
- Residual element content (as examples, phosphorus, sulfur, tin, antimony, and arsenic).
- Strength level as determined by heat treatment, with susceptibility increasing with increasing strength. This is likely to be an indirect effect on ductility, which generally decreases with increasing strength.
- Grain size: coarse-grain steels are more vulnerable than fine-grain steels.
- Manufacturing apparatus used to introduce the plastic strain. For example, various bending machines might produce bends with the same mean bend radius to outside diameter ratio (R/D) but not produce identical distributions of plasticity in the completed bend.
- Temperature at which the plastic work is introduced—that is, hot formed, intercritically formed, or cold formed.

- Strain level and manner of deformation. There is evidence that simple uniaxial strain, such as that produced by tube bending, is less deleterious than multi-direction strains (redundant working), such as those produced by upsetting, swaging, or flaring.
- Relationship of subsequent service to the creep range (that is, whether subsequent service is below or above the creep range).

After forming operations in fabrication of ferritic tubing, the options are (a) to place the material into service as formed, (b) to perform a subcritical heat treatment (with temperature below AC_1—this treatment is commonly called a *stress relief*), or (c) to anneal or normalize (possibly followed by a temper).

In the broad sense, forming temperatures can be classified as cold forming ($T \leq 0.3$ Tm), warm forming (0.3 Tm $< T \leq 0.5$ Tm), and hot forming ($T >$ 0.5 Tm), where *Tm* is the melting temperature on the absolute temperature scale [23]. The melting temperature for iron is 2788°F (1531°C), which equates to 3248°R (1804°K). Thus, cold forming of steel would be at temperatures below 514°F (268°C), warm working between 514°F and 1164°F (268°C and 629°C), and hot working above 1164°F (629°C). Although this definition is useful conceptually, it is not really appropriate for materials that undergo complex phase changes when they are cooled from melting temperature to room temperature.

A more useful delineation between cold and hot forming relates to the recrystallization temperature, at which cold forming occurs below the recrystallization temperature and hot forming involves recrystallization concurrent with the forming. The recrystallization temperature is then defined in relation to the lower transformation temperature.

In ASME Code for Pressure Piping B31 [24], paragraph 129.3.1, hot bending or forming is performed at a temperature above AC_1 minus 100°F (38°C), and cold bending or forming is performed at a temperature below AC_1 minus 100°F (38°C). Thus, using this definition for 2¼Cr1Mo steel with an AC_1 temperature of about 1480°F (804°C), the delineation between cold and hot working occurs at 1380°F (749°C). Rules are provided for post-forming heat treatment of piping in ASME B31.1, but these rules are not necessarily consistent with the usual practices for boiler tubing. Thus, Table 7-1, which has been distilled from several sources, is provided as guidance for post-forming heat treatment of bends in Grade 11 and 12 steel tubes. As a practical matter, intercritical forming is usually done toward the high end of the temperature range to take advantage of the lower strength while forming.

Table 7-1
Guidance on Post-Forming Heat Treatments for Bends in Grade 11 and 12 Tubes

Type of Forming	Forming Temperature (°F)	Bends R/D	Stress Relief Temperature (°F)	Comments
Cold Forming Below	≤1200	>3.0	Not required	
Recrystallization	≤1200	≤3.0	1200–1325	Common practice.
Temperature	≤1200	≤2.5	1200–1325	Limited practice.
Intercritical Forming	1200–1700	All	Anneal, normalize 1700°F minimum, or normalize and temperature 1200°F minimum.	Heat treatment is advised because of partially transformed microstructure.
Hot Forming	1700–1875	All	Not required unless hardness exceeds limits of procurement specification, then SR 1200–1325°F	Forming is in austenitizing range and cooldown produces normal microstructure but hardness may be too high.

°C = (5/9) x (°F-32)

Two additional issues need to be addressed relative to tube bending: wall thinning on the extrados and ovality. ASME Section I does not address either of these issues, whereas B31.1 treats both subjects [24]. In short, B31.1 requires that the wall thickness on the extrados must not be thinner than the minimum wall thickness calculated for a straight pipe of the same outside diameter. In Table 102.4.5 of B31.1, guidance is provided on the amount of thinning to be expected for R/D ratios from 3 to 6. In spite of the rationale provided by Section I for permitting wall thinning on the extrados in violation of the minimum calculated wall thickness in a straight pipe, it is good practice for a utility to impose requirements beyond the Code rules. A common practice is to require the wall thickness on the extrados to be at least 90% of that required for a straight tube, that is, to permit no more than a 10% violation of the minimum wall thickness due to thinning on the extrados.

On the subject of ovality for ferrous materials, in paragraph 104.2.1 of B31.1, a limited treatment is given for ovality. Ovality is defined as follows:

$$\text{Ovality} = 100(D_{max} - D_{min})/D$$

where

D_{max} = maximum measured diameter at any section of the bend
D_{min} = minimum measured diameter at the same section in the bend
D = the average measured outside diameter of the straight pipe before bending

The B31.1 requirement for bends with $R/D \geq 5$ and Schedule 40 thickness or greater is that the ovality must not exceed 8%. Reasonable ovality criteria for bent tubes that utilities can impose on the fabricator are as follows:

Ovality $\leq$ 8 % for $R/D \geq 5$
Ovality $\leq$ 10 % for $\{5 > R/D \geq 1.5\}$
Ovality $\leq$ 12 % for $R/D > 1.5$

7.2 Welding

7.2.1 Welding Processes and Consumables

These alloy steels are air-hardening and subject to cracking if not properly handled. Because of the hardenability conferred by the alloying elements present, the 1Cr½Mo and 1¼Cr½MoSi steels are classified as P No. 4, Grade No. 1 for welding and PWHT. To weld these tubes, it is necessary to use low hydrogen coated electrodes. Thus, for shielded metal arc welding (SMAW), an E8018-B2 electrode is typically used. A 250ºF (121ºC) minimum preheat is appropriate for thick joints (t > ½ in.) with high restraint and a minimum specified tensile strength in excess of 60 ksi. Welds in thinner sections can be made without preheat, but exemption from PWHT is usually contingent on a minimum preheat of 250ºF (121ºC). For gas tungsten arc welding (GTAW) or gas metal arc welding (GMAW), ER80S-B2 wire nominally matches the composition of Grades 12 and 11 and is used most often.

In Section I, when there is no exemption from PWHT for Grade 12 and 1¼Cr½MoSi steel in Table PW-39, the PWHT temperature is 1200ºF (649ºC) minimum for a time of 1 hour per inch of thickness with a minimum time at temperature of 15 minutes. Although Section I has no maximum temperature for PWHT, the rules of B31.1 require a range of 1200–1300ºF (649–704ºC) for P no. 4 materials.

Further information regarding welding of Grade 11 and 12 steels is given below; however, complete details are contained in applicable ASME codes (Section IX) and EPRI reports [25, 26].

7.2.2 Welding PWHT

PWHT is performed to relieve residual stresses introduced during fabrication or the welding operation. It also improves ductility and toughness of the weldment. With a few exceptions, PWHT is specified for low alloy steel weldments.

PWHT involves raising the temperatures of the complete weld joint slowly, holding it at a specified temperature for a defined period, and following that with slow cooling. Each step is critical and must follow the requirements of the established welding procedure specification (WPS) and Code.

It should be noted that the PWHT requirements differ slightly according to different Codes. Therefore, it is essential to determine the applicable Code and apply the proper PWHT requirements when conducting a repair. In the case of high-temperature piping, ASME B31.1 should be used.

A standard procedure should be prepared for the PWHT of weld joints. The procedure should specify the following details:

- Requirements of the various codes
- Guidance in selecting heating methods
- Installation of heating equipment: width of heating band, thermocouple attachment, and locations
- Heating and cooling cycle and hold time
- Quality assurance and documentation

For Grades 11 and 12, the requirements of B31.1 are 1300–1375ºF (704–746ºC) for 1 hour per inch (1 hour per 25 mm) for a nominal thickness of up to 2 in. (50.8 mm) and 2.25 hours for each additional inch (millimeter) over 2 in. (50.8 mm). It should be noted that ASME specifications indicate PWHT at a minimum of 1100ºF (595ºC). For most high-temperature applications, unless a specialist temperbead technique has been applied, this would be considered insufficient to properly temper the weld, and there would be a risk of low ductility creep failure.

Typical recommended PWHT requirements for high-temperature piping materials are as listed in Table 7-2.

Table 7-2
Recommended PWHT Requirements for High-Temperature Piping Materials

P Number	Holding Temperature
P1	1100–1200ºF (593–649ºC)
P3	1100–1200ºF (593–649ºC)
P4	1300–1375ºF (704–746ºC)

Holding time for P1, 3, 4, and 5 should be 1 hour per inch (1 hour per millimeter) for a nominal thickness up to 2 in. (50.80 mm) and 2.25 hours for each additional inch (millimeter) over 2 in. (50.80 mm). Holding time for Cr-Mo-V should be 1 hour per inch (1 hour per millimeter), with a 2-hour maximum.

For P1, 3, 4, and 5 weldments, the heating and cooling rate above 600ºF (316ºC) shall not exceed 600ºF (316ºC) per hour divided by half the maximum thickness of material in inches at the weld; however, in no case shall the rate exceed 600ºF (316ºC). For Cr-Mo-V weldments, the heating and cooling rate above 750ºF (399ºC) shall not exceed 450ºF (232ºC) per hour divided by the maximum thickness of material in inches (mm) at the weld; however, in no case shall the rate exceed 220ºF (104ºC) per hour.

7.2.3 Weld Procedure Selection

A written welding procedure qualified in accordance with ASME Section IX is required for pressure boundary welding. The purpose of the procedure qualification is to ensure that the weldment exhibits the required properties for the intended application. The requirements needed to qualify a welding procedure for pressure boundary components are specified in ASME Section IX, "Welding and Brazing Qualifications."

It is imperative that the correct welding procedure be chosen for the application. A welding procedure should consist of a WPS and a procedure qualification record (PQR). The WPS gives direction to the welders for making the production welds. Both essential and nonessential variables listed in ASME Section IX for the particular process(es) employed should be included on the WPS. The PQR should list the essential variables used to weld the test coupons and the test results.

7.2.3.1 P Numbers

To reduce the number of welding procedures, materials are grouped according to their base metal characteristics, such as composition weldability and mechanical properties. This grouping is known as the *P number*.

A complete list of material specifications and their corresponding P numbers can be found in the ASME Boiler and Pressure Vessel Code, Section IX, Table QW-422. A partial list of boiler materials is shown in Table 7-3. This table can be used to obtain the P number once a material

specification and grade have been identified. If the ASME specification is unknown but the nominal chemical composition has been determined by chemical analysis, the P number can be obtained by comparing the nominal chemical composition and corresponding P numbers.

Table 7-3
Summary of Designated Weld P Numbers for Selected Alloy Steels

P-Number	Nominal Composition	ASME Specification Number and Grade				
		Product Form				
		Tube	Pipe	Forging	Casting	Plate
1	Carbon Steel	SA-17BA,C,D SA-192 SA-21BA1, C	SA-53 SA-1068, C	SA-105 SA-181	SA-216WCA SA-216WCB	SA-285C SA-515GR 60, 70 SA-516GR 60, 70 SA-299
3	Carbon Molybdenum Chrome Molybdenum Manganese Molybdenum	SA-209T1 T1A, T1B SA-213T2	SA-335P1 SA-335P2	SA-185F1 SA-182F2	SA-217WC1	SA-204-A SA-387 Grade 2 SA-302B
4	1% to 1 ½ Chromium - ½% Molybdenum 1 ¾% to 2% Chromium - ½% Molybdenum	SA-213T11 T12 SA-213T3	SA-335P11, P12 SA-369FP11, FP12 SA-335P3 SA-369FP3b	SA-182F11, F12	SA-217WC6	SA-387 Grade 11, 12
5a	2 ¼% Chromium - 1% Molybdenum 3% Chromium - 1% Molybdenum	SA-213T22 SA-213T21	SA-335P22 SA-335P21	SA-182F22 SA-182F21	SA-217WC9	SA-387 Grade 22 SA-387 Grade 21
5b	5% Chromium – 1/% Molybdenum 9% Chromium - 1% Molybdenum 9Cr – 1 Mo – V – Cb – N	SA-213T5 SA-213T9 SA-213T91	SA-335P5 SA-335P9 SA-335P91	SA-182P5 SA-182P9 SA-182P91	SA-217C5 SA-217C12	 SA-387 Grade 91

The materials have been grouped by P number for welding purposes only. Under no circumstances should the grouping be used for material selection. For example, although SA-213 Grade T22 and SA-213 Grade T9 have the same P number, T22 should not be substituted when T9 is specified. Additionally, the P number grouping of materials should not be confused with the steel grade designation. For example, a typical pipe material is ASME SA-335 P2, which is a 0.5% Cr-0.5% Mo low alloy steel. In this case, the Grade P2 indicates the particular alloy content and is not related to the P number grouping. Examination of Table 7-3 shows that SA-335 P2 has a P number grouping of 3. Similarly, materials SA-335 P7 and P9 grades have a P number grouping of 5.

The identification of the P number for both parts to be welded is a critical first step in selecting the welding procedure. It is important that the materials to be joined are correctly identified and that the corresponding P numbers are accurately determined.

7.2.4 Weld Joint Preparation

7.2.4.1 Open Butt Joint

When a complete pipe or fitting has to be replaced, some form of joint preparation will be required to ensure proper fit-up and to provide adequate access for welding. It is not always appropriate to duplicate the groove design used during original fabrication because the replacement has to be performed *in situ* where access might be difficult and there are equipment restrictions. It is essential to select a weld joint configuration that will provide reasonable access for achieving acceptable weld quality but which does not require an excessive amount of welding time. Selecting a weld groove angle that is too wide will require an unnecessary amount of welding time.

Although the weld groove geometry is not an essential variable for the ASME Section IX WPSs that cover the commonly used GTAW and SMAW processes, it is recommended that standard weld joint preparations for butt welding be selected whenever possible.

The important features of a weld preparation are the following:

- Included angle
- Root opening
- Root face
- Radius at the root

Figure 7-1 shows the various elements in a typical weld joint end preparation. Both the included angle of the groove and the root opening directly affect the access of the welding electrode. The proper combination is needed to avoid a lack of sidewall fusion defects, which result if the weld groove is too narrow. If the weld groove is too wide, it will result in unnecessary welding. The root opening and the root face are critical in ensuring good root fusion without melting through. A too-wide opening and too-thin root face will usually result in excessive penetration and/or melt-through. An opening that is too narrow and root face that is too thick will result in lack-of-penetration defects.

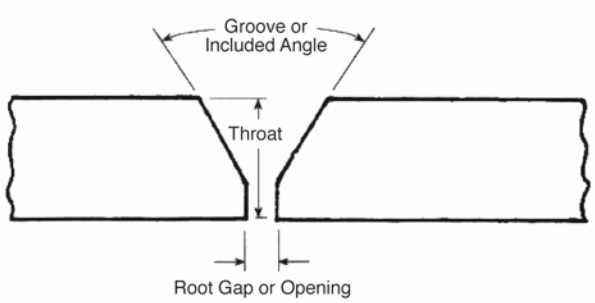

Figure 7-1
Groove Weld End Preparation Nomenclature

7.2.4.2 Compound V-Butt Joint

For thick-walled components, a compound V-groove or U-groove is usually selected. The wider opening at the bottom portion of the weld groove provides proper electrode manipulation for good fusion, whereas the narrower angles on the upper portion of the groove minimize welding time. Proper alignment of the inner diameter is essential for achieving an acceptable root. Counterboring might be necessary to remove ovality and to minimize inner diameter mismatch. The typical standard weld preparations that have been adopted by utilities are shown in Figure 7-2.

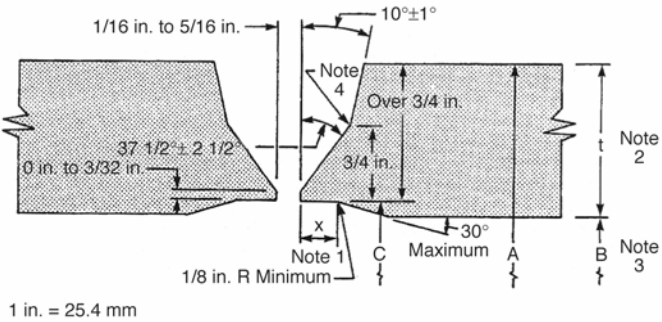

Notes:

1. Minimum depth of counterbore (X) shall be ½ inch or t, whichever is less. In no case shall the counterbore infringe on the minimum required wall thickness.

2. 2t = Specified Wall Thickness (Nominal or Minimum)
   t_{norm} = Nominal Wall Thickness
   t_{min} = Minimum Wall Thickness

3. A = Nominal Pipe O.D Inches
   B = Nominal Pipe I.D. Inches
   C = Counterbored I.D. at Weld End Prep

4. Inside corners within weld end preparation shall be slightly rounded.

Figure 7-2
Open Root Joint Details

7.2.5 Repair Pipe and Fitting Weld Repair and Replacement

There are various acceptable techniques for the repair of high-temperature piping. Most repairs to low alloy steels require high-temperature PWHT; in certain repairs, however, this is not always possible. Both ASME Section XI and the National Board Inspection Code (NBIC) permit special welding repair methods as alternatives to performing PWHT. Details can be found in NBIC Chapter III, Supplement 3. These techniques should be used only after careful engineering judgment and under the supervision of a welding engineer who is familiar with these techniques and the risk involved.

7.2.5.1 Localized Defect Removal: Weld Repair Required

A weld repair is necessary when the depth required to remove unacceptable defects results in the remaining wall thickness being below Code-acceptable limits. When unacceptable subsurface indications are found by ultrasonic testing (UT) and their removal results in the component being below the minimum wall thickness requirement, a weld repair must also be performed. As illustrated in Figure 7-3, the following are the steps for performing this type of weld repair:

1. Excavate the defect (surface indications will already be exposed; UT indications must be exposed).
2. Remove defects by grinding, gouging, or machining.
3. Surface-grind and verify defect removal by wet fluorescent magnetic particle inspection (MPI).
4. Perform weld repair.

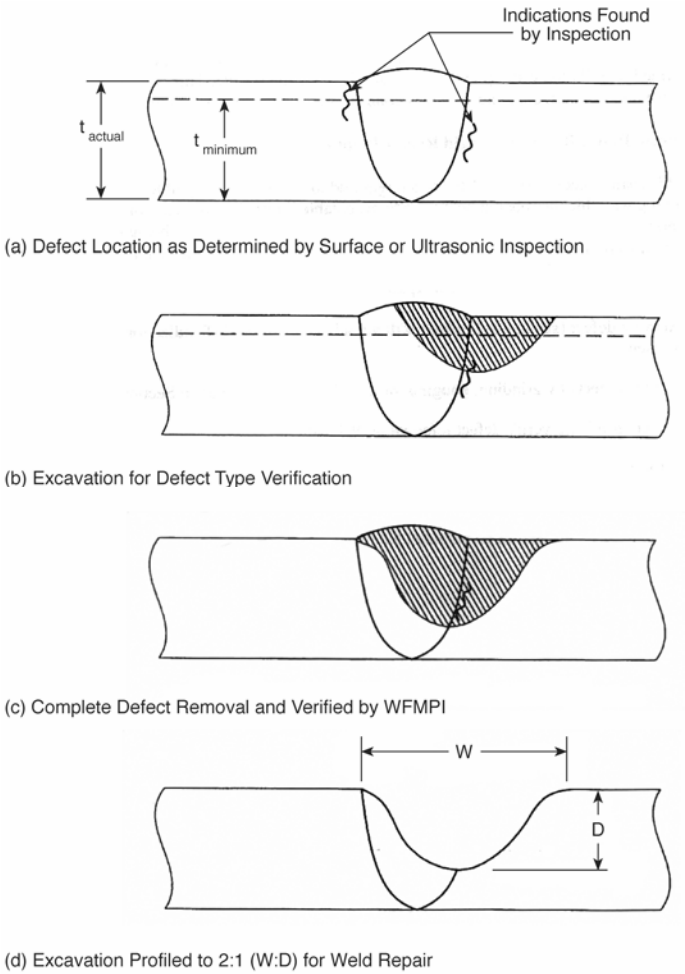

Figure 7-3
Excavations for Defect Type Verification and Local Weld Repair

Figure 7-4 illustrates the fill sequence for a cavity requiring a local weld repair.

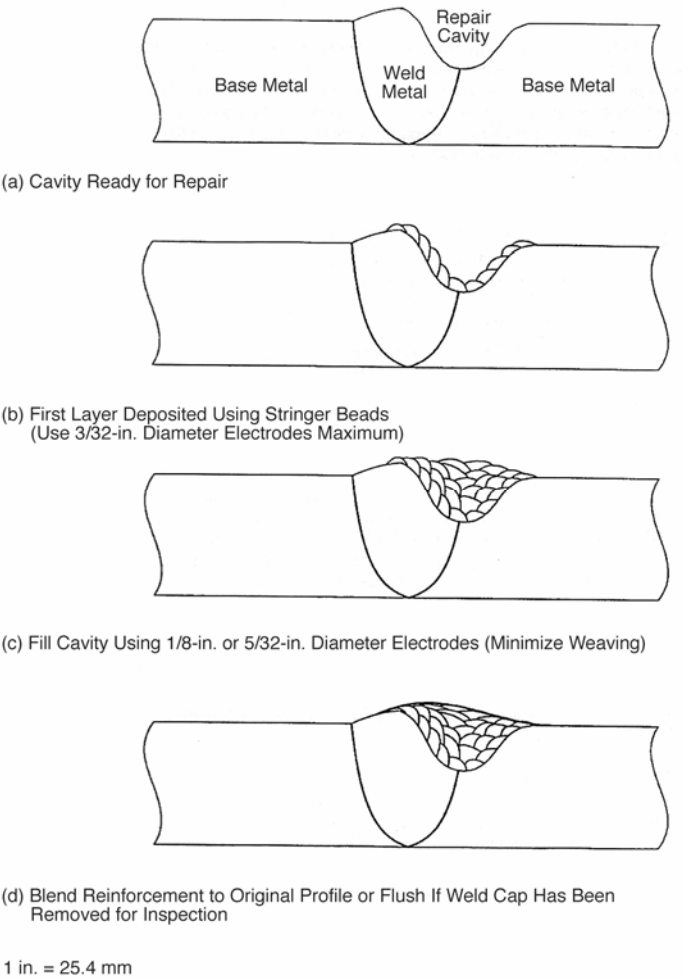

Figure 7-4
Cavity Fill Sequence for Local Weld Repair

Following a local repair, the area should be examined by magnetic particle testing (MT) and UT, and the inspection results of the localized repair should be recorded for future reference.

7.2.5.2 Repair of a Full Groove Excavation

The weld and HAZ regions shall be removed using an appropriate excavation method. Machining is strongly recommended when a full weld excavation is performed. Experience has shown that removing the material by machining provides economic, timing, and quality advantages. Preheat must be applied if gouging is used. Figure 7-5 illustrates a typical final shape of a cavity that is ready for rewelding. The profile of the cavity should be chosen to ensure complete removal of the HAZ and facilitate proper welding access. The final cavity shape should be kept in mind during excavation, and material removal should proceed accordingly.

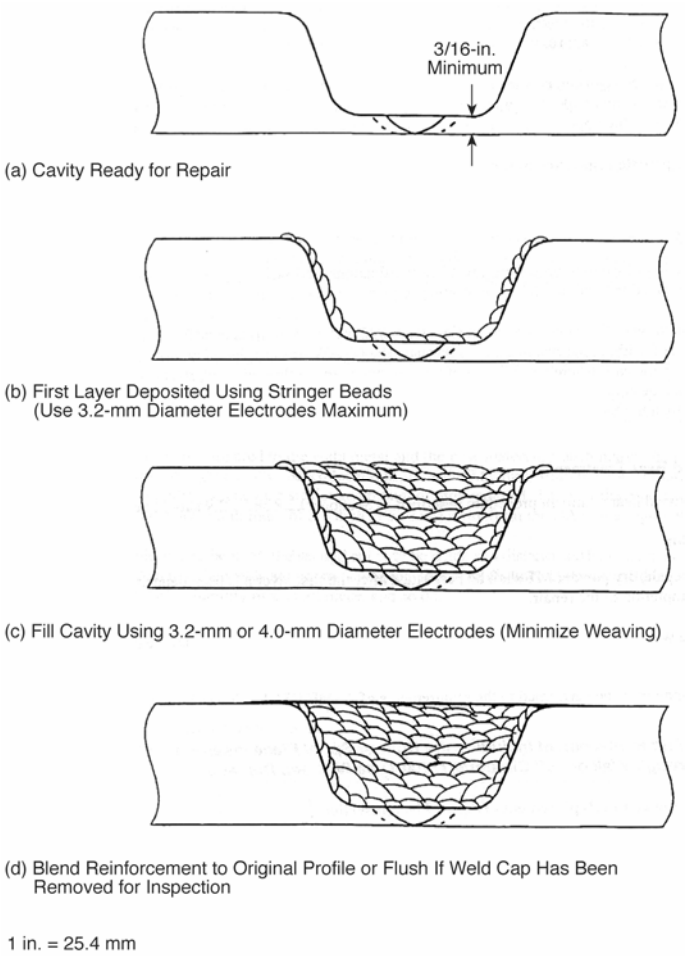

Figure 7-5
Cavity Fill Sequence for Full Weld Replacement

When approximately two-thirds of the thickness of the weldment has been removed, periodic ultrasonic wall thickness measurements should be performed on the remaining root thickness to ensure that the final thickness of approximately 3/16 in. (4.76 mm) remains intact.

If the excavation has been performed by arc gouging, the entire cavity must be ground to remove scale to a minimum depth of 1/16 in. (1.59 mm). The cavity must be blended to smooth transitions with the upper weld cavity edges and the lower corners to ease weld deposition.

MPI must be performed on the entire joint preparation prior to the commencement of welding.

7.2.5.3 Repair of Type IV Creep Damage

When Type IV damage or cracking has been identified on high-temperature piping components and the severity of the damage is found to warrant the replacement of the weld metal and HAZ, a special defect removal and weld preparation technique is recommended.

In the case of Type IV creep damage, it is essential that the entire HAZ be removed because damage occurs at the intercritical zone between the HAZ and the base metal and experience suggests that the greatest levels of damage can occur below the surface. The profile of the original weld preparation should be determined from manufacturer drawings and/or welding procedure and verified by macro-etching to determine the extent of the excavation. An excavation within an arbitrary distance of 5/8 in. (15.88 mm) from the fusion line has been found to be adequate to ensure complete removal of the damaged HAZ. Another important feature of this type of repair is that the excavation does not penetrate through the entire wall, thus minimizing fit-up and root gap opening problems. Nevertheless, it is important to verify complete removal of the defect by nondestructive examination methods, such as visual inspection, MPI, or dye penetrant examination.

7.2.5.4 Temperbead Repair

The cavity should be filled using electrodes no greater than 5/32 in. (3.10 mm) in diameter. Preferably, smaller diameter electrodes should be used for the first layers of repairs on base material. Use a stringer technique and minimize weaving as much as possible for the first two layers. This technique is similar to the temperbead technique used for avoiding PWHT. Although this technique is not a Code requirement for repair welding with a full PWHT, it is good practice because it is known to reduce the hardness of the HAZ and optimize its microstructure. The cavity should be filled completely to just above the existing profile of the surrounding base material. The capping pass should then be ground back to blend in uniformly with the surrounding base material.

8
REFERENCES

1. *Metallurgical Guidebook for Fossil Power Plant Boilers.* EPRI, Palo Alto, CA: 2006. 1011912.
2. R. Viswanathan, "Damage Mechanisms and Life Assessment of High Temperature Components." ASTM International, West Conshohocken, PA: 1989.
3. *The Handbook of Comparative World Steel Standards, Second Edition.* DS67A. ASTM International, West Conshohocken, PA: 2002.
4. J. D. Parker, H. J. Westwood, and G. C. Stratford, "Weldment Creep Damage in 1.25Cr0.5Mo Steel." *Proceedings of the International Conference on Plant Life Management.* (October 1992.) pp. 4-21–4-30.
5. P. J. Alberry and W. K. C. Jones, "Diagram for the Prediction of Weld Heat Affected Zone Microstructure." *Metals Technology,* Vol. 4, No. 4, pp. 360–364 (1977).
6. H. J. Westwood , M. A. Clark, and D. Sidey, "Type IV Cracking in a CrMo Steam Line." Presented at the International Conference on Creep and Fracture of Engineering Materials and Structures. The Institute of Metals, London, UK, 1990. p. 621.
7. J. Nutting, "The Structural Stability of Low Alloy Steels for Power Plant Applications." Electric Power Institute conference: London, UK (1999). *Advanced Heat Resistant Steels for Power Generation.* pp. 12–30.
8. J. H. Hollomon and L. D. Jaffe, "Time-Temperature Relations in Tempering Steel." *Trans. AIME,* Vol. 162, pp. 223–249 (1945).
9. F. R. Larson and J. Miller, "A Time-Temperature Relationship for Rupture and Creep Stresses." *Trans. ASME,* Vol. 74, p. 765 (1952).
10. *Life Assessment of Boiler Pressure Parts: Volume 2: Materials Properties.* EPRI, Palo Alto, CA: 1994. TR-103377-V2.
11. G. V. Smith, "Supplemental Report on the Elevated Temperature Properties of Chromium Molybdenum Steels." ASTM Data Series, DS 6S1, ASTM International, West Conshohocken, PA: 1971.

12. R. Viswanathan, “Strength and Ductility of 1¼Cr-1Mo Steels in Creep at Elevated Temperatures.” *Metals Technology,* June 1974, pp. 284–294.

13. *A Review of High Temperature Performance Trends and Design Rules for Cr-Mo Steel Weldments.* EPRI, Palo Alto, CA: 1998. TR-110807.

14. European Creep Collaborative Committee, data sheets, 1999.

15. *Remaining Life of Boiler Pressure Parts, HAZ Models.* EPRI, Palo Alto, CA: 1998. RP 2253-1.

16. *Creep Crack Growth Behavior in Power Plant Boiler and Steam Pipe Steels.* EPRI, Palo Alto, CA: 1987. RP 2253-10.

17. *Embrittlement of Components in Fossil Fueled Power Plants.* EPRI, Palo Alto, CA: 2003. 1004515.

18. Guidance on Methods for Assessing the Acceptability of Flaws in Metallic Structures (Incorporating Amendment 1). British Standards Institution, London, UK: 1999. BS 7910:1999.

19. K. Takamatsu, Y. Otoguro, K. Shinozuka, and K. Hashimoto, *Journal of Iron and Steel.* Institute of Japan, Vol. 17, pp. 129–138 (1979).

20. *Boiler Tube Failures: Theory and Practice.* EPRI, Palo Alto, CA: 1996. TR-105261.

21. I. G. Wright and B. A. Pint, “An Assessment of the High-Temperature Oxidation Behavior of Fe-Cr Steels in Water Vapor and Steam.” Paper no. 02377 presented at the NACE Corrosion/2002 conference, Denver, CO (April 2002).

22. A. Fry, S. Osgerby, and M. Wright, “Oxidation of Alloys in Steam Environments—A Review.” National Physical Laboratory Report MATC(A) 90, 2002.

23. John H. Schey, *Introduction to Manufacturing Processes, Third Edition.* McGraw-Hill, New York, NY: 2000.

24. ASME Code for Pressure Piping, B31: B31.1 Power Piping, 2004. American Society of Mechanical Engineers, New York, NY: 2004.

25. *State-of-the-Art Weld Repair Technology for High Temperature and Pressure Parts Repair Guideline: Volumes 1 and 2*. EPRI, Palo Alto, CA: 1996. TR-103592-V1 and TR-103592-V2.

26. *Guideline on Fossil Boiler Field Welding*. EPRI, Palo Alto, CA: 2003. 1004701.

Export Control Restrictions

Access to and use of EPRI Intellectual Property is granted with the specific understanding and requirement that responsibility for ensuring full compliance with all applicable U.S. and foreign export laws and regulations is being undertaken by you and your company. This includes an obligation to ensure that any individual receiving access hereunder who is not a U.S. citizen or permanent U.S. resident is permitted access under applicable U.S. and foreign export laws and regulations. In the event you are uncertain whether you or your company may lawfully obtain access to this EPRI Intellectual Property, you acknowledge that it is your obligation to consult with your company's legal counsel to determine whether this access is lawful. Although EPRI may make available on a case-by-case basis an informal assessment of the applicable U.S. export classification for specific EPRI Intellectual Property, you and your company acknowledge that this assessment is solely for informational purposes and not for reliance purposes. You and your company acknowledge that it is still the obligation of you and your company to make your own assessment of the applicable U.S. export classification and ensure compliance accordingly. You and your company understand and acknowledge your obligations to make a prompt report to EPRI and the appropriate authorities regarding any access to or use of EPRI Intellectual Property hereunder that may be in violation of applicable U.S. or foreign export laws or regulations.

The Electric Power Research Institute (EPRI), with major locations in Palo Alto, California; Charlotte, North Carolina; and Knoxville, Tennessee, was established in 1973 as an independent, nonprofit center for public interest energy and environmental research. EPRI brings together members, participants, the Institute's scientists and engineers, and other leading experts to work collaboratively on solutions to the challenges of electric power. These solutions span nearly every area of electricity generation, delivery, and use, including health, safety, and environment. EPRI's members represent over 90% of the electricity generated in the United States. International participation represents nearly 15% of EPRI's total research, development, and demonstration program.

Together...Shaping the Future of Electricity

Program:

Fossil Materials and Repair

Printed on recycled paper in the United States of America

1013358

Electric Power Research Institute
3420 Hillview Avenue, Palo Alto, California 94304-1338
PO Box 10412, Palo Alto, California 94303-0813 USA
800.313.3774 • 650.855.2121 • askepri@epri.com • www.epri.com